

THE EFFECTS OF ROUGHNESS ON HEAT TRANSFER
FROM OPEN CHANNEL FLOW

A THESIS

Presented to

The Faculty of the Graduate Division

by

Michael David Moss

In Partial Fulfillment

of the Requirements for the Degree

Master of Science in Civil Engineering


Georgia Institute of Technology

March, 1976

T-264
24-3

THE EFFECTS OF ROUGHNESS ON HEAT TRANSFER
FROM OPEN CHANNEL FLOW

Approved:


Chairman

Date Approved by Chairman: 3/15/76

ACKNOWLEDGMENTS

The author wishes to thank Dr. Paul G. Mayer, without whose unending care and advice, both technical and personal, the completion of this thesis would not have been possible. For his suggestion of the topic and his work in successfully obtaining research funds for the project, the author is deeply indebted.

The members of the reading committee, Dr. George M. Slaughter and Dr. John M. Hamrick, are gratefully acknowledged for their review of the thesis.

The office of Water Research and Technology is to be thanked for its financial support of this project.

The financial assistance of the School of Civil Engineering is gratefully acknowledged.

Special thanks go to Mrs. Margaret S. Fain for a careful review of the manuscript and for the typing of this thesis.

The laboratory efforts were ably carried out by numerous students in the School of Civil Engineering. Particularly noteworthy contributions were made by Robert P. Stevens (M.S. Civil Engineering, 1974), Paula A. McGuire (Bachelor of Civil Engineering, 1974), and Richard A. Johann (Bachelor of Civil Engineering, 1975).

In order that the text of this thesis could be used as a report to the Office of Water Research and Technology, special permission was granted by the Division of Graduate Studies to vary the thesis requirements in pagination, margins, and headings.

TABLE OF CONTENTS

	Page
ACKNOWLEDGMENTS.....	ii
LIST OF FIGURES.....	v
LIST OF TABLES.....	vii
LIST OF SYMBOLS.....	viii
SUMMARY	xi
CHAPTER	
I. INTRODUCTION.....	1
Description of the Problem	
Purpose and Scope of the Investigation	
II. REVIEW OF THE LITERATURE.....	4
III. MODELING CONSIDERATIONS.....	10
Physical-Mathematical Model	
Estimating Heat Transfer from Atmospheric and Surface	
Conditions	
Boundary Layer Approach to Estimate the Difference	
between Surface and Bulk Water Temperatures	
Effects of Flow and Momentum Turbulence	
Determination of Viscous Boundary Layer Parameters	
Turbulent Diffusion Boundary Layer for Heat Transfer	
Near a Surface	
Determination of Friction Velocity in the Heat Flux	
Equation	
IV. EXPERIMENTAL APPARATUS AND PROCEDURES.....	33
Apparatus	
Procedures	
V. LABORATORY RESULTS AND ANALYSES.....	37
Laboratory Results	

TABLE OF CONTENTS

	Page
Comparison of Free-convection Equation with Still Water Data	
Application of Prediction Equation to Smooth and Rough Channel Runs	
VI. APPLICATION OF THE RESULTS.....	63
Utilizing the Models	
Effect on Cooling Pond Design	
VII. CONCLUSIONS AND RECOMMENDATIONS.....	72
Conclusions	
Recommendations	
REFERENCES.....	75

Patented
FLAVOR BOND
25% COTTON FIBER
U S A

LIST OF FIGURES

<u>Figure</u>	<u>Title</u>	<u>Page</u>
1	Relative Increase in Saturation Water Vapor Pressure per Degree Centigrade Rise in Temperature.....	13
2	Near Interface Water Temperature Profiles for Quiescent and Highly Turbulent Flows.....	15
3	Sketch of Conduction Layer Model for Bouyant Convection.....	24
4	Schematic View of Experimental Apparatus.....	34
5	Photograph of Experimental Apparatus.....	35
6	Still Water Cooling Data, Run Number 1.....	49
7	Observed and Predicted Heat Transfer Rates for Still Water, Run Number 1.....	50
8	Still Water Cooling Data, Run Number 2.....	51
9	Observed and Predicted Heat Transfer Rates for Still Water, Run Number 2.....	52
10	Control Volume for Conservation of Thermal Energy in Flume.....	55
11	Predicted vs. Observed Heat Transfer in Roughened Channel.....	57
12	Predicted vs. Observed Heat Transfer in Smooth Channel.....	58
13	Histogram of Roughened Channel Surface Temperature Depression.....	60
14	Histogram of Smooth Channel Surface Temperature Depression.....	61
15	Model Water Surface Heat Transfer in Roughened Channel with Various Velocities.....	65

LIST OF FIGURES

<u>Figure</u>	<u>Title</u>	<u>Page</u>
16	Model Surface Temperature Depression in Roughened Channel with Various Velocities.....	66
17	Model Water Surface Heat Transfer in Smooth Channel with Various Velocities.....	67
18	Model Surface Temperature Depression in Smooth Channel with Various Velocities.....	68

LIST OF TABLES

Table		Page
1.	Experimental Data - Smooth Channel.....	38
2.	Experimental Data - Rough Channel, Series A.....	40
3.	Experimental Data - Rough Channel, Series B.....	41
4.	Experimental Data - Rough Channel, Series E.....	42
5.	Experimental Data - Still Water.....	44
6.	Experimental Data - Still Water.....	46

Permanized
PLOVER BOND
25% COTTON FIBER
U.S.A.

LIST OF SYMBOLS

A	coefficient in equation for heat transfer due to flow turbulence, dimensionless
a	free convection coefficient in Dalton equation, $\text{cal cm}^{-2} \text{sec}^{-1} \text{mbar}^{-1}$
Area, Area _*	surface area of cooling pond, cm^2
b	turbulent convection coefficient in Dalton's equation, $\text{cal cm}^{-2} \text{sec}^{-1} (\text{cm/sec})^{-1} \text{mbar}^{-1}$
b ₁ , b ₂ , b ₃	polynomial coefficients in water vapor pressure versus temperature equation
c	coefficient in equation for heat transfer due to Bénard convection, dimensionless
C _B	Bowen's constant, $\text{millibars} \cdot ^\circ\text{C}^{-1}$
c _p	heat content of water per unit mass, $\text{cal gm}^{-1} \cdot ^\circ\text{C}^{-1}$
d	water depth, cm
D	thermal diffusivity, $\text{cm}^2 \text{sec}^{-1}$
E	evaporation rate, $\text{gm cm}^{-2} \text{sec}^{-1}$
e _a	atmospheric vapor pressure, millibars
e _s	saturation vapor pressure at water surface, millibars
g	acceleration of gravity, cm sec^{-2}
g _s	temperature depression function for still water
g _f	temperature depression function for flowing water
h	heat transfer per unit temperature difference, $\text{cal cm}^{-2} \text{sec}^{-1} \cdot ^\circ\text{C}^{-1}$
h(t)	heat transfer as a function of time for still water

$H_1, H_2,$	upstream, downstream, and surface heat transfer in flume
H_s	control volume, cal sec^{-1}
k	thermal conductivity, $\text{cal cm}^{-2} \text{sec}^{-1} (^\circ\text{C/cm})^{-1}$
k	roughness height, cm
k_n	kinematic heat transfer coefficient, cm sec^{-1}
k_m	mass transfer coefficient, cm sec^{-1}
ℓ	characteristic mixing length in Nusselt and Rayleigh numbers, cm
ℓ	near surface mixing length, cm
L	latent heat of water vaporization, cal gm^{-1}
L	length of flume test section, cm
M	molecular weight of water vapor, gm mole^{-1}
Nu	Nusselt number, dimensionless
P	atmospheric pressure, millibars
q	heat transfer per unit surface area, $\text{cal cm}^{-2} \text{sec}^{-1}$
Q	volumetric flow rate of water, $\text{cm}^3 \text{sec}^{-1}$
R	hydraulic radius, cm
R	universal gas constant
R	ratio of absolute water surface temperature to air temperature
Ra	Rayleigh number, dimensionless
S	flume slope
T_a	air temperature, $^\circ\text{C}$
T_s	water surface temperature, $^\circ\text{C}$
T_s	water surface temperature, turbulent mixing, $^\circ\text{C}$
T_v	virtual temperature, $^\circ\text{C}$
T_w	mean water temperature, bulk temperature, $^\circ\text{C}$
V	average velocity of water in flume, cm sec^{-1}
v_o	friction velocity, cm sec^{-1}

v_y	eddy velocity near surface, cm sec^{-1}
w	width of flume, cm
W	wind speed, cm sec^{-1}
α	thermal diffusivity, $\text{cm}^2 \text{sec}^{-1}$
β	thermal expansivity, $^{\circ}\text{C}^{-1}$
δ	diffusion layer thickness, cm
δ_l	thermal conduction layer thickness, cm
δ_o	viscous boundary layer thickness, cm
λ	thickness of layer damped by surface tension, cm
ν	kinematic viscosity, $\text{cm}^2 \text{sec}^{-1}$
ν_{turb}	effective eddy viscosity, $\text{cm}^2 \text{sec}^{-1}$
ρ	mass density, gm cm^{-3}
ρ_a	atmospheric vapor density, gm cm^{-3}
ρ_s	saturation vapor density at water surface, gm cm^{-3}
σ	Stefan-Boltzmann constant, $\text{cal cm}^{-2} \text{sec}^{-1} \text{K}^{-4}$
σ	surface tension, gm sec^{-2}
τ	boundary shear stress, $\text{gm sec}^{-2} \text{cm}^{-1}$
Φ_c	water surface conduction and convection heat loss, $\text{cal cm}^{-2} \text{sec}^{-1}$
Φ_e	water surface evaporative heat loss, $\text{cal cm}^{-2} \text{sec}^{-1}$
Φ_l	water surface long-wave radiation heat loss, $\text{cal cm}^{-2} \text{sec}^{-1}$
Φ_s	water surface short-wave radiation heat loss, $\text{cal cm}^{-2} \text{sec}^{-1}$

SUMMARY

The purpose of this study was to establish quantitatively the effect of turbulence on heat dissipation in open channels. The study investigated systematically factors which affect heat transfer from open channel flow. Thus, an attempt was made to combine the thermodynamic and hydrodynamic phenomena in order to obtain design parameters. An examination was made of channel roughnesses as a means of additional mixing and hence of additional thermal transfer.

The laboratory study showed the quantitative increase in evaporative cooling as a consequence of increased turbulent mixing in open channel flow and suggests artificially roughened channels as an alternate means of accomplishing the rejection of excess industrial heat into the environment.

The theoretical study provided a means for the application of the study results to the design of open channels as an alternate means of dissipation of excess industrial heat.

CHAPTER I

INTRODUCTION

Description of the Problem. Water temperatures are an important criterion for the environmental assessment of water quality. The temperature of water bodies affects their suitability for human consumption and for industrial uses. Water temperatures also affect directly a stream as an aquatic habitat for important ecological food chains which include desirable fish species, aquatic predators and ultimately man.

In view of the prospective development of very large industrial complexes including central power generating stations, both fossil-fuel and nuclear powered, the need exists for the assimilation by the environment of very large amounts of rejected heat. Under the increased pressure by regulatory agencies for enforcement of water quality standards, the cooling of heated condenser water is a common requirement before such liquid effluents may be discharged into the environment.

As an indicator of water quality in streams and lakes, water temperature has a unique and complex role. Although elevated water temperatures are not undesirable a priori, the mere fact of an increased temperature is presumed to be detrimental to stream and lake biota, particularly to higher life forms. Perhaps even more significantly, temperature is the one physical parameter which affects most of the other major indicators of water quality, physical, chemical, and biological. An increase in water temperature has the potential for significantly altering the hydrodynamic and thermodynamic characteristics

of a stream or lake. Another physical effect is the super-linear increase in the water vapor pressure with an increase in water temperature and a subsequent increase in surface evaporation causing possibly adverse water losses and elevated local humidity in addition to the advantageous effect of evaporative cooling. A major physio-chemical effect of elevated water temperatures is the lowering of the saturation concentrations of dissolved gases, most notably dissolved oxygen. Increased chemical reaction rates may also cause an increased degradation of stream quality. The biological effects include increased growth rates of oxygen depleting organisms and thus increased dissolved oxygen depletion rates. In light of the various and complex consequences of increased thermal energy in streams, the addition of heat in excess of that normally encountered in a stream or lake has been defined as thermal pollution by the Federal Water Pollution Control Administration (FWPCA) (9).

According to the FWPCA, almost one-half of the water used in the United States is for cooling and condensing by the power and manufacturing industries. Of this, almost 80 percent is used by the electric power generating industry. As the generating capacity of this industry continues to increase, the need exists for the assimilation by the environment of large amounts of excess heat. The water quality standards enforced by national and state regulatory agencies require that significant reductions of thermal discharges to natural waters must be made, commensurate with the assimilative capacities of the receiving water bodies. Methods of economical on-site reduction of temperatures for water discharges from industrial plants are therefore a subject of

considerable interest.

Coupled with the lack of understanding of the complex interactions of increased temperature with other in-stream processes is the inability to accurately predict the effects of hydrodynamic flow processes on evaporative cooling. The lack of understanding of the transfer process at the water surface, especially in the case of strongly heated water, is also a significant drawback in the proper design of cooling ponds. Some studies have been reported which attempted to quantitize the increased evaporative cooling due to the buoyancy added by the heated water. The causes and effects of internal mixing on the surface temperature as the main driving force of the evaporative cooling process have not been studied.

Purpose and Scope of the Investigation. It is the objective of this study to investigate the internal mixing processes, both in an otherwise quiescent case and in cases of turbulence induced by the mean flow of water and by added channel roughnesses. It is proposed that the natural thermal convection currents near a water surface, not previously described in the literature as relevant to evaporative cooling, are indeed significant. Accordingly, evaporative cooling may be considerably enhanced by induced flow turbulence much as in the case of a stirred cup of coffee. The net effect of increased turbulent mixing is to be shown to yield a significant increase in the overall cooling rate by evaporation from water surfaces.

Experimental and theoretical investigations are to be conducted with the aim of quantitizing the effect of turbulent mixing on water surface temperatures and on evaporative cooling.

CHAPTER II

REVIEW OF THE LITERATURE

The basic aspects of heat transfer from a water surface to the atmosphere can be conveniently grouped into four categories. These are net solar (short-wave) radiation exchange, net long-wave radiation exchange, evaporative (latent) heat loss, and conduction and convection (sensible) heat loss. Paily, Macagno & Kennedy (26) present a comprehensive review of techniques for the estimation of the short-wave component of heat exchange. Paily, et al., also present a thorough review of techniques for estimating the long-wave radiation component.

The net long-wave exchange is itself composed of three separate components, the long-wave radiation from the water surface, radiation from the atmosphere, and the subsequent reflection of this component by the water surface. Long-wave radiation from the water can be computed using the Stefan-Boltzmann law of radiation modified for the emissivity of the water surface which was estimated by Anderson (1). The Stefan-Boltzmann law is also used to estimate long-wave radiation from the atmosphere with certain modifications. The reflectance of the water surface must be considered, and an estimate of it is given by Anderson, who also proposed an expression for the emissivity of the atmosphere.

By far the most difficulty in a predictive model is presented by the evaporative cooling term along with the sensible heat loss term. Except for the most recent investigations into the evaporative heat

loss from water bodies, most studies considered water temperatures in the naturally occurring range, with stable atmospheric thermal gradients. Investigations mostly considered conditions in lakes and reservoirs when hydraulic mixing did not influence evaporation. The present authors have been unable to find any substantial reports on the effects of flow induced turbulence and internal mixing on heat transfer from open channels.

Dalton (7) was the first investigator to identify the driving force of evaporation from a wet surface into the atmosphere and described this process in 1802. This process, usually referred to as Dalton's law, is the net exchange of vapor molecules from the saturated surface and from the moist atmospheric environment. The driving force is then the difference between the saturated vapor pressure at the water surface and the ambient vapor pressure in the atmosphere. Dalton's law is the statement of the proportionality of the evaporative flux to this vapor pressure difference.

As Dalton's law only identified the main driving force of evaporation, it remained the task of others to determine the coefficient of proportionality. A variety of formulae have been proposed using a linear function of the wind velocity as this coefficient, notably those of Kohler (16), Marciano and Harbeck (22), and Rohwer (29). Harbeck (22) noted a slight variation in the coefficient with water surface area. These formulae were determined from field and laboratory studies of lakes and reservoirs without internal mixing and with stable atmospheric thermal gradients.

The first investigator to develop an adequate formula for evaporation from heated water bodies into atmospheres with unstable thermal gradients was the Russian investigator, Shulyakovskiy (32). Using the heat-mass transfer analogy, he developed a proportionality coefficient as a function of wind velocity and of the difference between the water surface temperature and atmospheric temperature. Ryan, Harleman, and Stolzenbach (30) using the definitive data of Fishenden and Saunders (10) on heat transfer from heated horizontal flat plates into air have recently presented a modified form of Shulyakovskiy's equation.

In addition to the heat lost as latent heat of evaporation, there is a sensible heat loss through molecular conduction and convection. Bowen (4) in 1926 introduced a technique for determining the ratio of sensible heat loss to evaporative heat loss using the analogy between heat and mass transfer. This technique has been widely accepted and is almost universally applied when using the evaporation formulae mentioned above. Anderson concluded from his Lake Hefner studies that except for the case of small driving force, the so-called Bowen-ratio approach is quite reliable. Applying the Bowen-ratio approach when using formulae such as those of Shulyakovskiy, and Ryan, et al., which are already based on the heat-mass transfer analogy would seem somewhat redundant, as will be discussed later in this report.

Nearly all of the formulae proposed in the literature included a driving force which assumed that the surface temperature can be approximated by the mean water temperature averaged over the depth. The exception is that of Shulyakovskiy's formula, in which he suggested using a method of determining the temperature depression at the surface.

Methods for calculating this temperature drop between the bulk water temperature and the surface temperature have not been found in the literature for flowing water.

Quiescent water, that is, water in which turbulent convection from the bulk of the water into the surface is not influenced by mean flow conditions has been the object of much research. However, the research has been conducted in a different area, namely that of convection in a confined horizontal layer of liquid with a vertical temperature gradient. This phenomenon was first reported and discussed by Bénard (3) in 1900. Since then, interest in the phenomenon has continued to grow. Most of this work considered confined liquid layers from 0.5 - 15 centimeters thick, heated from below and generally cooled from above. After the thermal gradient reached a critical value, it became unstable and convective motion began which carried denser cooler water from the top to the warmer bottom. Depending on the configuration of the confining boundary, this motion occurred as a distinct pattern of convective cells or rolls in which warm water rose in the center of the cells and cool water descended at the outer edges. Bénard convection has been studied largely as a stability phenomenon with emphasis on the critical values for different convection modes and on the types and effects of cellular rolls which can be induced. Notable among these studies are those of Malkus (20), Krishnamurti (17), (18), and Willis and Deardorff (33).

The reported studies which are more important to this study, however, are those which relate the overall vertical temperature difference to the heat transfer rate through the surface layer. The data of

O'Toole and Silveston (25) covered the significant range of conditions and substantially validated the empirical expression derived from dimensional analysis and from analytical stability studies. The O'Toole and Silveston expression related the Nusselt number to the cube root of the Rayleigh number. The same relation was used by Fishenden and Saunders (10) in their study on heat transfer from heated horizontal plates into air. The studies of Fujii and Imura (11), Chu and Goldstein (6), and Hollands, Raithby, and Konicek (14) confirmed this relationship within reasonable limits. Hollands, et. al., developed a formula which related the coefficient in this relationship for the total temperature drop across the fluid layer to the coefficient appropriate when considering the temperature drop at only one bounding surface. This expression of Hollands, et. al., was used in the present study as the surface temperature depression function for still water.

Reports on the effects of mean flow mixing on the turbulent motion near the surface and subsequently on the surface temperature depression and on over-all heat transfer from a water surface have not been found. However, in the study of dissolution of gases at flowing surfaces, Levich (19) has developed a theoretical Prandtl-von Kármán-type mixing length model near the surface of laminar and turbulent flows. The Levich equation was based upon the "universal" velocity distribution in the turbulent case and contains the channel "friction velocity" as a term. In this study the work of Keulegan (15) relating the friction velocity, hydraulic radius, and channel roughness to mean velocity was used to extend Levich's expression to the case of uniform flow in open channels. Mayer and Moss (23) have presented a mathematical model

which attempted to quantify the effect of turbulent mixing in open channel on the surface temperature depression and on evaporative cooling.

Permanized
PLOVER BOND
25% COTTON FIBER

CHAPTER III

MODELING CONSIDERATIONS

Physical-Mathematical Model. Prediction of heat transfer rates across a free water surface into air is necessarily complex due to the presence of two coupled boundary layers at the interface. The mechanism of transfer on the atmospheric side of the interface has been widely investigated and predictive tools are available. Investigation of the transfer structure within the water surface layer has centered around an analysis of the phenomenon, observed first by Bénard, of closed convection cells in a thin layer of liquid with controlled heating from below and controlled cooling from above. This problem was treated from the standpoint of stability and convection mode transitions, and much data is available today for accurate prediction of heat transfer rates in a liquid layer with fixed upper and lower surfaces. Some work has been done to extend this information to the case of a liquid layer with a free upper surface (i.e., absence of the "no-slip" condition at the upper surface) and it appears that this extension was successful. Experimentation covered the range of layer thicknesses from $\sim 0.5 - 15.0$ cm and Rayleigh numbers of up to 10^9 . Although the results were generally independent of layer thickness, they covered the range of environmentally significant conditions.

Very little information has been found from investigations into the effects of water flow regimes upon the evaporation rates from the flowing surface. This lack of information is due in large part to the

fact that mixing patterns become an important factor only at liquid temperatures greatly elevated above ambient, whereas much of the reported work of estimating evaporative heat fluxes has been involved with natural water surfaces with temperatures in the environmental range or heated water bodies such as cooling ponds in which flow is not significant.

The present investigation was directed toward developing an adequate coupling of the water and air boundary layers in order to predict heat transfer rates due to evaporative cooling. This involves essentially the estimations of the surface temperature depression below the bulk water temperature due to vertical heat transfer. As can be observed from the form of the water vapor pressure curve as a function of temperature and from noting that the near-surface vapor pressure is the main driving force of heat transfer, this surface-to-bulk temperature difference becomes more and more important as the bulk temperature of the water is increased over ambient air temperatures and as the heat transfer rate into the atmosphere becomes larger, both of which occur simultaneously in environmental situations.

The effect of the difference in temperatures between the water surface and bulk fluid can be demonstrated. Noting that at elevated water temperatures the water surface vapor pressure is much larger than the ambient vapor pressure, or $e_s > e_a$, the driving force for evaporative cooling is $(e_s - e_a)$, and the heat transfer rate due to evaporation will be approximately proportional to e_s . Using a nonlinear regression technique, an accurate fit to the water vapor pressure curve was made using the functional form

$$e_s = \exp (b_1 + b_2 T_s + b_3 T_s^2) \quad (1)$$

The coefficients were determined to be

$$b_1 = 1.6001, \quad b_2 = 0.067295, \quad b_3 = -0.00017475$$

for e_s in millibars and T_s in $^{\circ}\text{C}$. The rate of change of vapor pressure with respect to water surface temperature is

$$\frac{de_s}{dT_s} = (b_2 + 2b_3 T_s) e_s \quad (2)$$

and the relative change in the driving force with a change in surface temperature is approximated by the difference equation

$$\frac{\Delta e_s}{e_s} = (b_2 + 2b_3 T_s) \Delta T_s \quad (3)$$

The percentage changes in evaporative heat transfer per degree Centigrade change in water surface temperature from the temperature of the bulk of fluid is then simply $b_2 + 2b_3 T_s$. This term is plotted against T_s in Figure 1.

In turbulent flow, the bulk inertial forces are increasingly larger than the surface forces at increasingly larger levels of turbulence. Under these conditions of turbulent flow, the bulk inertial forces drive liquid eddies from the main motion continually into the surface layer, thus reducing surface stagnation and enhancing the mass-transfer rate, and simultaneously enhancing the rate of evaporative cooling. With increased turbulent mixing in open channel flow, turbulent eddy motion drives the hotter fluid of the main stream into the surface

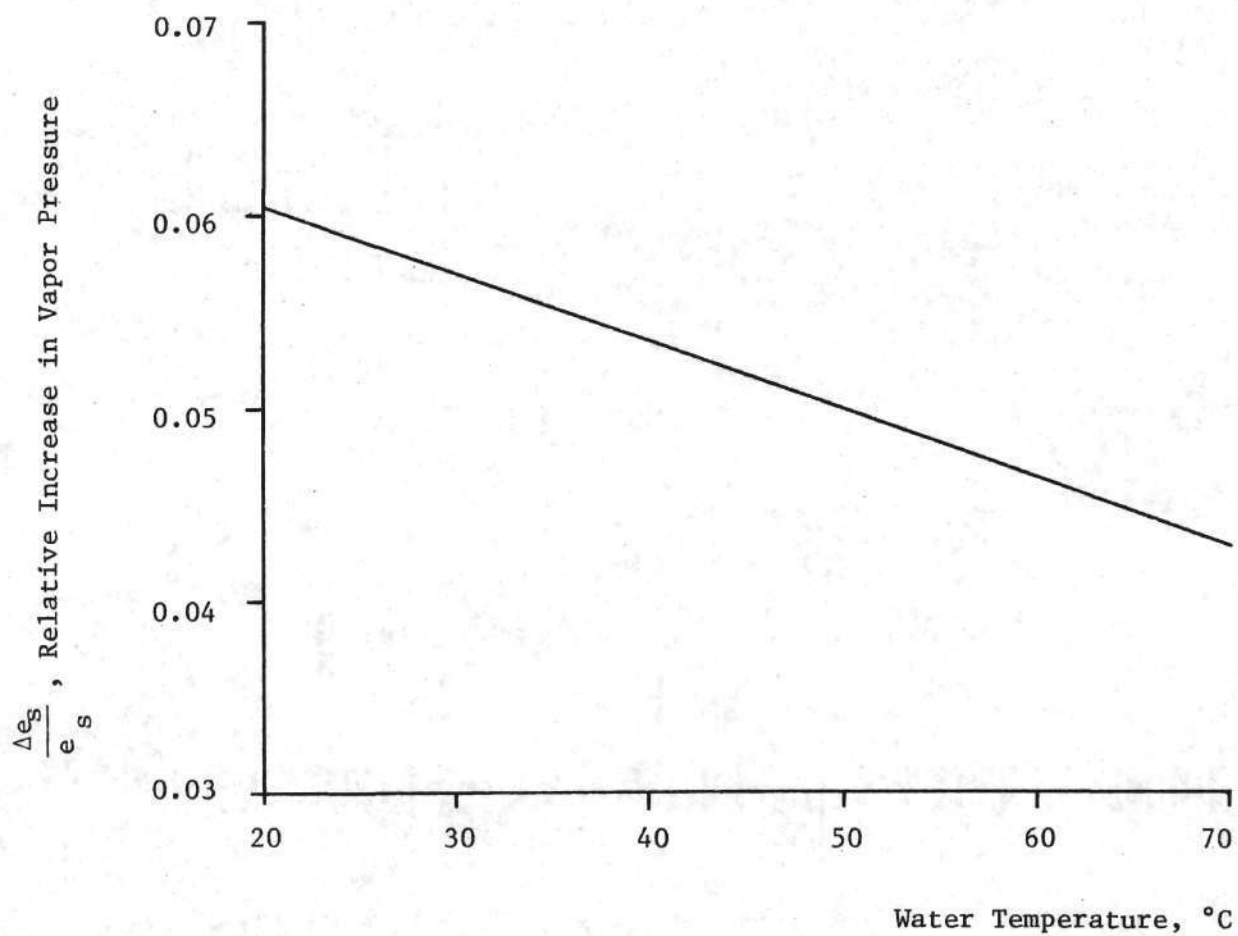


Figure 1. Relative Increase in Saturation Water Vapor Pressure per Degree Centigrade Rise in Temperature

layer. Thus, the water surface temperature is increased from its natural value, T_s , to a forced convection value, T'_s . This reduction of the difference between the bulk water temperature, T_w , and the surface temperature, T_s , causes a significant increase in the temperature difference between the water surface and the ambient air, ΔT . The quantitative evaluation of this process is presented later on. Figure 2 shows the significant aspects of the effect of turbulent mixing on water surface temperatures in open channel flow.

Estimating Heat Transfer from Atmospheric and Surface Conditions. Heat transfer from a free water surface can be separated into four distinct components, short-wave radiation exchange (ϕ_s), long-wave radiation exchange (ϕ_l), conductive (convective) transfer (ϕ_c), and evaporative transfer (ϕ_e). The short-wave radiation exchange in a laboratory study can be conveniently neglected. Long-wave exchange is a function of the water surface and air temperatures and the water vapor content of the atmosphere. The formula proposed by Anderson, neglecting cloud cover, is used here and is expressed as

$$\phi_l = 0.97 \sigma (T_s + 273)^4 - (0.74 + 0.0049 \cdot e_a) \sigma (T_a + 273)^4 \quad (4)$$

where σ is the Stefan-Boltzmann constant, T_s is the water surface temperature in $^{\circ}\text{C}$, T_a is the air temperature in $^{\circ}\text{C}$, and e_a is the ambient water vapor pressure in millibars.

Conductive (convective) losses are usually predicted through the Bowen ratio concept, that is, the conductive (convective) transfer is assumed to be proportional to the heat transfer due to latent heat of vapor mass convection. This ratio is evaluated from

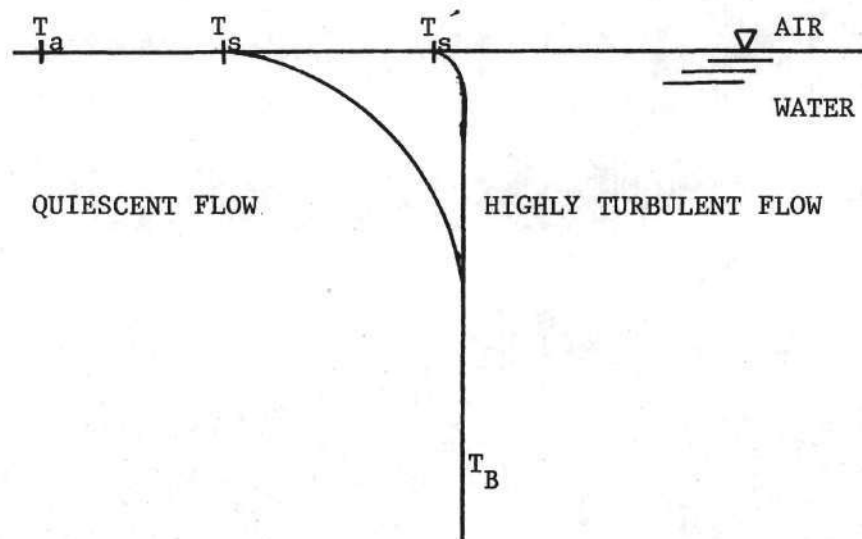


Figure 2. Near Interface Water Temperature Profiles for Quiescent and Highly Turbulent Flows

$$\Phi_c / \Phi_e = C_B (T_s - T_a) / (e_s - e_a) \quad (5)$$

where C_B is Bowen's constant, e_s is the saturation vapor pressure at the water surface temperature, and T_a and e_a are evaluated at the same specified height above the water surface.

Calculation of the heat transfer due to evaporative cooling is conventionally based on empirical expressions of the form

$$\Phi_e = (a + bW)(e_s - e_a) \quad (6)$$

where a and b are empirical constants and W is the wind velocity across the water surface. For near-ambient water temperatures, the largest contribution to Φ_e is through turbulent convection due to wind. Thus, Φ_e is sensitive to the constant b with varying values of wind speed and good estimates have been made of this coefficient. At elevated values of the water surface temperature, the predominant contribution to Φ_e is made by the buoyancy effect of the heated air and water vapor near the surface, a variable effect which is not adequately described by the constant, a . This buoyant term, a , can be estimated accurately through the use of the analogy between heat and mass transfer, as proposed by Shulyakovskiy and later refined and improved by Ryan, who used the definitive data of Fishenden and Saunders on buoyant heat transfer from horizontal plates. The development of this buoyant term as presented by Ryan, et al., is given here since a similar approach was used in the present study and because it represented some of the basic framework used in the analysis of the surface water layer regions.

Fishenden and Saunders investigated the heat transfer from heated

horizontal square plates in air in both the laminar and turbulent regimes. The plates were large enough so the end effects became negligible. In the turbulent regime, the data were correlated in non-dimensional form as

$$Nu = 0.14 Ra^{1/3} \quad (7)$$

where Nu is the Nusselt number, or the ratio of total heat transfer to conducted heat transfer, and is equal to

$$Nu = \frac{h\ell}{k}$$

and the Rayleigh number is

$$Ra = \frac{g\beta\Delta T\ell^3}{\alpha \nu}$$

where ℓ is the characteristic length,

h is the heat transfer rate per °C, temperature difference,

α is the thermal diffusivity,

k is the thermal conductivity,

β is the thermal expansivity,

g is the acceleration of gravity,

ν is the kinematic viscosity, and

ΔT is the bulk temperature difference.

Thus,

$$\frac{h\ell}{k} = 0.14 \left(\frac{g\beta\Delta T\ell^3}{\alpha \nu} \right)^{1/3}$$

or

$$h = 0.14k \left(\frac{g\beta\Delta T}{\alpha\nu} \right)^{1/3} \quad (8)$$

Since $k = \rho c_p \alpha$

where ρ is the density, and

c_p is the specific heat at constant pressure, the heat transfer rate becomes

$$h = 0.14 \rho c_p \alpha \left(\frac{g\beta\Delta T}{\alpha\nu} \right)^{1/3}$$

or

$$h = 0.14 \rho c_p \left(\frac{\alpha^2 g\beta\Delta T}{\nu} \right)^{1/3} \quad (9)$$

and the convection-conduction transfer, $\Phi_c = h \cdot \Delta T$ is given by

$$\Phi_c = 0.14 \rho c_p \left(\frac{\alpha^2 g\beta\Delta T}{\nu} \right)^{1/3} \Delta T \quad (10)$$

The kinematic heat transfer coefficient, $k_h = \frac{\Phi_c}{\rho c_p \Delta T}$ then becomes

$$k_h = 0.14 \left(\frac{\alpha^2 g\beta\Delta T}{\nu} \right)^{1/3} \quad (11)$$

This empirically derived expression for the heat transfer coefficient can be used in estimating mass transfer coefficient, k_m , by using the analogy which states that $k_m = k_h$. Thus, the total evaporation rate, E , becomes

$$E = k_m (\rho_s - \rho_a) \quad (12)$$

where ρ_s and ρ_a are the water vapor densities at the water surface and in the ambient air. Converting from mass to pressure differences, the heat transfer due to evaporation, $\Phi_e = EL$, where L is the latent heat of

vaporization, can be expressed as

$$\Phi_e = 0.14 \frac{LM}{R} \left(\frac{\alpha^2 g \beta \Delta T}{v} \right)^{1/3} \left(\frac{e_s}{T_s} - \frac{e_a}{T_a} \right) \quad (13)$$

where M is the molecular weight of water (M = 18.0 g/mole), R is the universal gas constant, and temperature is in absolute units. Since the transfer analogy does not take into account the effect of a large concentration of water vapor at the boundary, the above expression is multiplied by $P/(P - e_s)$, where P is the total atmospheric pressure. This then gives the expression for heat transfer due to convection of latent heat as

$$\Phi_e = 0.14 \frac{LM}{R} \left(\frac{\alpha^2 g \beta \Delta T}{v} \right)^{1/3} \left(\frac{P}{P - e_s} \right) \left(\frac{e_s}{T_s} - \frac{e_a}{T_a} \right) \quad (14)$$

This expression differs from that given by Ryan, et al., in that local temperatures are used in the gas law for converting from density to pressure differences instead of a single mean temperature, and the bouyant effect of the water vapor is included in the driving force. This seemed necessary in this study because larger temperature differences were considered.

The derivation of the pressure correction term $P/(P - e_s)$ is a modification of Hinze's discussion of analogies in turbulent transport. The derivation in Hinze was in terms of local gradients at the boundary. It was modified and used here for bulk transfer equations in order to assure a closer analogy to the heat transfer process.

Setting the near surface temperature ratio

$$\frac{T_s}{T_a} = r$$

the following expression is obtained

$$\phi_e = 0.14 \frac{LM}{RT_s} \left(\frac{\alpha^2 g \beta \Delta T}{v} \right)^{1/3} \left(\frac{P}{P-e_s} \right) (e_s - re_a) \quad (15)$$

The calculation of the empirically determined coefficient term was made by Fishenden and Saunders by using fluid properties at a temperature midway between T_s and T_a and this approach was followed in this study.

Since the evaporative heat transfer was computed using an analogy to the conduction-convection transfer process, it seemed more consistent to use the value of ϕ_c determined in order to evaluate ϕ_e instead of using the Bowen ratio approach. In keeping with the previous discussions, a virtual temperature difference, ΔT_v , was used throughout instead of the absolute temperature difference, ΔT . The virtual temperature of moist air is defined as the temperature of dry air which has the same thermal energy as the moist air and is computed from

$$T_v = T / (1 - 0.378 \frac{e_a}{P})$$

where temperatures are in °K, and e_a is the vapor pressure of the moist air in the same units as P , the atmospheric pressure. The final derived expression for the sum of natural convection and conduction-convection transfer is

$$\phi_c + \phi_e = 0.14 \left(\frac{g \alpha^2 \beta \Delta T_v}{v} \right)^{1/3} \left\{ \frac{PLM}{(P-e_s)RT_s} (e_s - re_a) + \rho c_p \Delta T_v \right\} \quad (16)$$

Boundary Layer Approach to Estimate the Difference between Surface and Bulk Water Temperatures. An intuitive analysis of the thermal condition beneath a cooling water surface with a sufficiently high cooling rate

shows the presence of two distinct regions. At the surface, one can imagine a thin stable layer where heat is transferred solely through molecular conduction. Beneath this layer in the bulk portion of the fluid, the stability of the surface breaks down and convective density currents and, for flowing water, bulk flow turbulence are persistent enough to maintain a nearly uniform distribution of temperature. This intuitive picture has indeed been quantitatively validated in the rather extensive literature on experimental and mathematical investigations of what has become known as Bénard convection in horizontal layers of liquid.

Investigation of heat transfer through horizontal layers of liquid has thus centered around the two aspects of the phenomenon. Most of the work during the first part of this century has dealt with the determination, both analytically and experimentally, of the point at which convective transfer becomes active and conductive stability breaks down. The most significant research as it relates to the present investigation, is that relating the Nusselt number to the Rayleigh number for the convective region. The empirical relationship proposed is similar to that for horizontal heated plates in air, and the asymptotic relationship for high Rayleigh numbers substantially was validated as

$$\text{Nu} = c\text{Ra}^{1/3} \quad (17)$$

Below the onset of instability, the relationship is simply

$$\text{Nu} = 1 \quad (18)$$

The exponent on the Rayleigh number near the critical region has been reported consistently as less than $1/3$ but never less than about $.278$. However, in the present study, the Rayleigh numbers were always high enough to be near asymptotic range, and the one-third exponent was used.

The empirically derived heat transfer formulae relating Nu to Ra can be used to determine the theoretical thermal layer thickness by assuming that all transfer through a thin layer is conductive. For the stable range where $Nu = 1$, the layer thickness is simply the total thickness of the fluid. For the unstable convective mode, the thermal layer thickness is determined from

$$Nu = cRa^{1/3} \quad (19)$$

or

$$\frac{h\ell}{k} = c \left(\frac{g\beta\Delta T\ell^3}{\alpha\nu} \right)^{1/3} \quad (20)$$

and

$$\Delta T = \frac{\alpha\nu}{g\beta} \left(\frac{h}{ck} \right)^3 \quad (21)$$

This gives the convective temperature difference. To compute the conductive layer thickness, δ_ℓ , it was assumed that $Nu = 1$ which gives

$$\frac{h\delta_\ell}{k} = 1 \quad (22)$$

For the unstable range, the coefficient c of Equation 19 could be estimated by

$$c = \frac{q}{k\Delta T} \left(\frac{\alpha \nu}{g\beta\Delta T} \right)^{1/3} \quad (23)$$

where q is the heat transfer rate per surface area, and ΔT is the surface to bulk temperature difference.

Fishenden and Saunders' data for air were fitted with a value of c equal to 0.14. Fujii and Imuro report a value of 0.13 for water. These values, however, are for experiments in which the heated surface was located at a solid wall and thus a no-slip condition existed at the boundary. In the case of the surface of a water layer exposed to air, this no-slip condition is somewhat, though not entirely, relaxed. The surface tension forces maintain a tight molecular surface layer which is only seldom broken into by the thermally induced convection. Vorticity and continuous motions were observed at the surface during convective transfer, which would seem to aid in intensifying the magnitude of the convective rolls. Due to this lessened surface resistance to the convective motions in the case of a free surface boundary condition, the value of the coefficient, c , was expected to be somewhat larger than 0.13, although this value was nevertheless used in this study.

As reported in the literature, this value of c was determined using single heated plates in an extensive fluid environment. For a bounded horizontal layer, the situation is somewhat different. Hollands, et al., used a conduction layer approach and they discussed a modification of the constant c in order to use the temperature drop across one conduction layer instead of the total fluid layer. This involves using a value of one-half the total temperature drop across the complete fluid layer in the Nusselt-Rayleigh relationship. Using a value of c

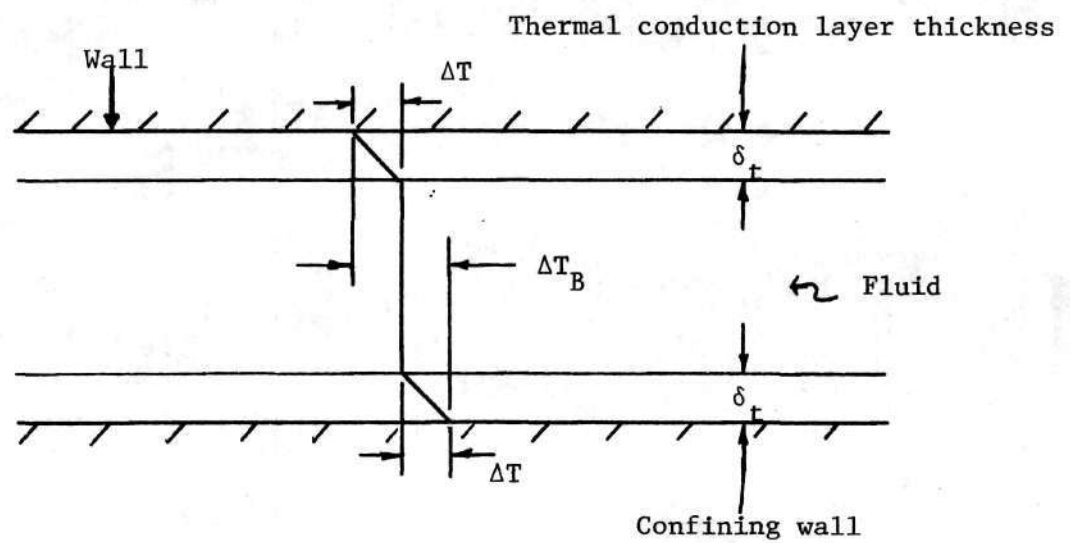


Figure 3. Conduction Layer Model
for Buoyant Convection
(after Hollands, et al.(14))

equal to 0.13, the Equation 19 then becomes

$$Nu = \frac{c}{2^{4/3}} Ra^{1/3} = 0.0555 Ra^{1/3} \quad (24)$$

Visually, the conduction layer model conceptualizes the thermal distribution in the fluid layer as depicted in the Figure 3. The coefficient, $\frac{c}{2^{4/3}}$, is used in the equation along with ΔT_B , the bulk temperature difference. The case of a conduction region on the lower as well as the upper side of a fluid layer with equal heat flow through each layer (steady state), is essentially the same as using an unmodified value of c and the single conduction layer temperature difference, ΔT .

In the case of a cooling container of fluid, there will be no lower conduction layer and heat transfer is strongly inhibited only at the upper surface. The equation used will then contain the coefficient $\frac{c}{2^{4/3}} = 0.0555$, where $c = 0.13$. The temperature differences ΔT and ΔT_B will be the same in this case and the Equation 24 is then based on the cooling surface temperature depression.

Effects of Flow and Momentum Turbulence. The net effect of flow turbulence is to reduce the thermal layer thickness by adding to the mixing produced by density currents in the fluid. At high Rayleigh numbers, the mixing due to thermal gradients may be much larger than that produced by lower levels of flow turbulence, but flow turbulence should generally add to the mixing already present. To determine the added effect of flow mixing on the thermal layer thickness, it is seen from Equations 20 and 22 that

$$\delta_L = \frac{1}{c} \left(\frac{\alpha v}{g \beta \Delta T} \right)^{1/3} = \frac{1}{c^{3/4}} \left(\frac{\alpha v q}{g \beta k} \right)^{1/4} \quad (25)$$

and δ_q is approximately inversely proportional to c when q does not vary much. Mixing is then detected in Equation 17 by a larger value of the coefficient c . Since the heat transfer q is also an increasing function of the surface temperature, a thinner thermal layer produces larger values of q .

For high Reynolds number flows, the effect of thermally induced turbulent mixing is not important and the thermal layer thickness is entirely dependent upon mixing due to turbulent momentum exchange. Thus, the Nusselt number is independent of the Rayleigh number in this case and is a function of the Reynolds number with perhaps some small variation with Prandtl number, $P_r = \alpha/\nu$, the ratio of thermal diffusivity, α , to kinematic viscosity, ν .

In the completely turbulent range, as defined in the literature on hydraulics, the wall roughness becomes predominant in determining the level of turbulent mixing in open channel flow. Since an increase in the wall roughness was also expected to greatly influence the heat transfer from the surface of the water, experiments were conducted in this study to determine this effect. An analytical analysis of the problem was also made. The procedure followed was quite similar to the approach of Prandtl in analyzing the turbulent boundary layer along a flat plate. For the case of a free-surface boundary, the approach needed to be modified. This free surface problem had been considered by Levich in his study on turbulent transport in the surface region of thin liquid films. Levich's approach has been modified and used in this study for the case of open-channel flow.

Determination of Viscous Boundary Layer Parameters. The boundary

condition for a free-surface boundary layer approximation is similar to the condition at the boundary for turbulent flow over a stationary flat plate. In both cases, the magnitude of the turbulent eddy velocity contributing to turbulent mixing, v_y , must vanish at the boundary. In the case of a flat plate, v_y vanishes due to the viscous "no-slip" condition at a solid surface. At the free-surface v_y must also be zero, but for another reason. Surface tension forces associated with the liquid surface maintain the integrity of the surface with a force not easily overcome by turbulence momentum. A non-vanishing v_y is perhaps possible at very large Froude numbers where the surface itself becomes unstable, a condition which was not studied here since it presented other difficulties, such as spray generation and air entrainment.

Even though the same boundary condition must hold for v_y as with the flat plate, the mean velocity profile is quite different. As previously explained, at a free surface the condition of zero shear stress must hold. This, of course, means that in the near-vicinity of the surface the mean velocity gradient must vanish and a uniform "mean" velocity persists locally throughout the surface boundary layer. It was assumed in the following development that turbulent mixing was strong enough so that the value of the velocity near the surface was equal to the mean flow velocity over the channel cross-section.

In order to approximate the boundary layer behavior, it is assumed that the distance beneath the surface within which viscous forces are active is small and equal to λ . The predominance of the viscous forces in this region is made possible solely by the surface tension forces and is diminished as the energy of the mainstream turbulence eddies

become larger. Denoting the velocity corresponding to the mainstream turbulence eddies as v_o , which is approximated by the so-called friction velocity, and letting σ represent the surface tension, λ will be on the order of $\sigma/\rho v_o^2 = \frac{\sigma}{\tau}$, where τ is the shear stress per unit area of solid flow surface. Since the mean velocity is constant throughout the surface layer, the local eddy velocity, v_y , is on the order of y , the distance from the surface, until y equals λ at which point v_y becomes and remains equal to v_o . It should be noted that this is different from the quadratic increase found in the case of a solid boundary where the mean flow velocity is not constant but varies linearly with distance from the wall.

The characteristic Prandtl mixing length, ℓ , or eddy size, is also important in explaining the transport properties in turbulent flow. In the free surface case, the variation of the mixing length is much the same as v_y and the approximation $\ell \sim y$ is valid for the local mixing length within the boundary layer.

The eddy viscosity, in the turbulent portion of the fluid can be expressed as

$$v_{\text{turb}} = v_y \cdot \ell \quad (26)$$

which is in keeping with the classical mixing length theory where v_y and ℓ are the local eddy velocity and mixing length. Substituting their values into Equation 26 gives

$$v_{\text{turb}} = \frac{v_o y^2}{\lambda} \quad (27)$$

To determine the thickness of the viscous sublayer, δ_o , it should

be noted that at a distance δ_o from the surface, the effective viscosity becomes equal to the viscosity of the fluid, ν , and thus

$$\nu = \frac{\nu_o \delta_o^2}{\lambda} \quad (28)$$

from which is obtained

$$\delta_o = \left(\frac{\nu \lambda}{\nu_o} \right)^{1/2} = \left(\frac{\nu \sigma}{\rho \nu_o} \right)^{1/2} \quad (29)$$

The viscous sublayer thickness is, of course, not important in terms of describing the velocity profile since there is substantially no velocity gradient in the sublayer at the surface.

Turbulent Diffusion Boundary Layer for Heat Transfer Near a Surface. In

the case of fluids for which the thermal Prandtl number is significantly larger than 1, the diffusion boundary layer thickness will be smaller than the viscous sublayer thickness. It is in this diffusion boundary layer that the controlling resistance to thermal transport is to be found. Within the layer, heat flows solely through the mechanism of conduction. Outside the layer, the temperature of the fluid is equal to the bulk temperature. Within the layer, the temperature varies linearly from the bulk temperature to the temperature at the surface. Thus, once the diffusion layer thickness, δ , is determined, the heat flux through the layer can be computed from the simple conduction equation

$$q = \rho c_p \frac{D \cdot \Delta T}{\delta} \quad (30)$$

where q is the heat transfer rate in terms of energy per area, D is the diffusion constant for heat and ΔT is the difference in temperature

between the surface and bulk of the fluid.

To estimate the value of the heat diffusion boundary layer thickness, it should be recalled that in completely turbulent flow, the eddy diffusion constant for heat transfer is of the same order of magnitude as the eddy viscosity, which gives the approximating equation

$$D_{\text{turb}} = \nu_{\text{turb}} \quad (31)$$

In the proximity of the viscous surface boundary layer, this becomes

$$D_{\text{turb}} = \frac{\nu_o y^2}{\lambda} \quad (32)$$

At a value of $y = \delta$, it is seen that $D_{\text{turb}} = D$ is the value of the fluid property. Thus, at $y = \delta$

$$D = \frac{\nu_o \delta^2}{\lambda} \quad (33)$$

and therefore

$$\delta = \left(\frac{D\lambda}{\nu_o} \right)^{1/2} \quad (34)$$

Substituting Equation 34 into the heat flux equation gives

$$q = \rho c_p \left(\frac{\rho D}{\sigma} \right)^{1/2} \nu_o^{3/2} \Delta T \quad (35)$$

Determination of Friction Velocity in the Heat Flux Equation. The friction velocity, ν_o , is defined as $\nu_o = \sqrt{\tau/\rho}$, where τ is the shear stress on the wetted perimeter. In the case of uniform open channel flow, this becomes

$$\nu_o = \sqrt{gRS} \quad (36)$$

where R is the hydraulic radius and S is the slope of the channel. The well-known Chezy formula for the mean velocity of flow in open channels is

$$V = C \sqrt{RS} \quad (37)$$

which gives the friction velocity in terms of the Chezy coefficient and the mean velocity as

$$v_o = \frac{\sqrt{g}}{C} V \quad (38)$$

From this relationship, if the Chezy coefficient is known, substitution into the heat flux equation gives an expression for the heat flux in terms of fluid properties and the mean flow velocity, assuming as before, that the mean channel velocity, V , persists into the surface layer. For a rough channel, an expression for the average flow velocity in open channels based on the universal logarithm velocity profile in turbulent flow is

$$V = v_o (6.25 + 2.5 \ln (R/k)) \quad (39)$$

where k is the roughness height. The Chezy coefficient can then be expressed as

$$\frac{C}{\sqrt{g}} = 6.25 + 2.5 \ln (R/k) \quad (40)$$

and

$$v_o = V/2.5 \ln (12.18 R/k) \quad (41)$$

Substituting Equation 41 into the heat flux equation gives

$$q = \rho c_p \left(\frac{\rho D}{\sigma} \right)^{1/2} (2.5 \ln (12.18 R/k))^{-3/2} v^{3/2} \Delta T \quad (42)$$

It should be noted that since relative magnitudes were considered in determining this functional relationship, Equation 42 is more appropriately a proportionality. The heat flux can then be expressed as

$$q = \frac{\rho c_p A}{(2.5 \ln (12.18 R/k))^{3/2}} \left(\frac{\rho D}{\sigma} \right)^{1/2} v^{3/2} \Delta T \quad (43)$$

where A is a coefficient to be determined experimentally.

Patented
 PLOVER BOND
 25% COTTON FIBER
 U.S.A.

CHAPTER IV

EXPERIMENTAL APPARATUS AND PROCEDURES

Apparatus. The experimental apparatus consisted of a recirculatory flow system as shown schematically in Figure 4. Figure 5 is a photograph of the experimental smooth-walled flume as seen from the upstream end. The head bay consisted of a three-quarter-inch thick plywood box some two feet wide, four feet long and three feet high. A bell-mouth shaped entrance preceded a 24-foot long wooden flume. The flume was eight inches wide and had side walls eight inches in height. The flume was undergirded by a 8-inch aluminum channel and was supported by three leveling jacks. The flume terminated in a wooden tail bay which consisted of a plywood box some two feet wide, eight feet long and three feet high.

Water was supplied by a 2-inch line and recirculated by means of a centrifugal pump. The flow rates in the flume were controlled by a valve in the return line and were measured by means of a calibrated orifice meter. The water temperatures were elevated by means of a 50-foot long one-half inch diameter copper pipe heat exchanger which was inserted into the head bay and which was supplied with live steam. The steam flow rates were controlled by a valve in the condensate line. The condensate flow rates were measured by means of a rotameter.

Procedures. The laboratory studies were conducted basically in three groups of experiments. These groups were the experiments with heated water flowing in the smooth-walled flume, the experiments with heated

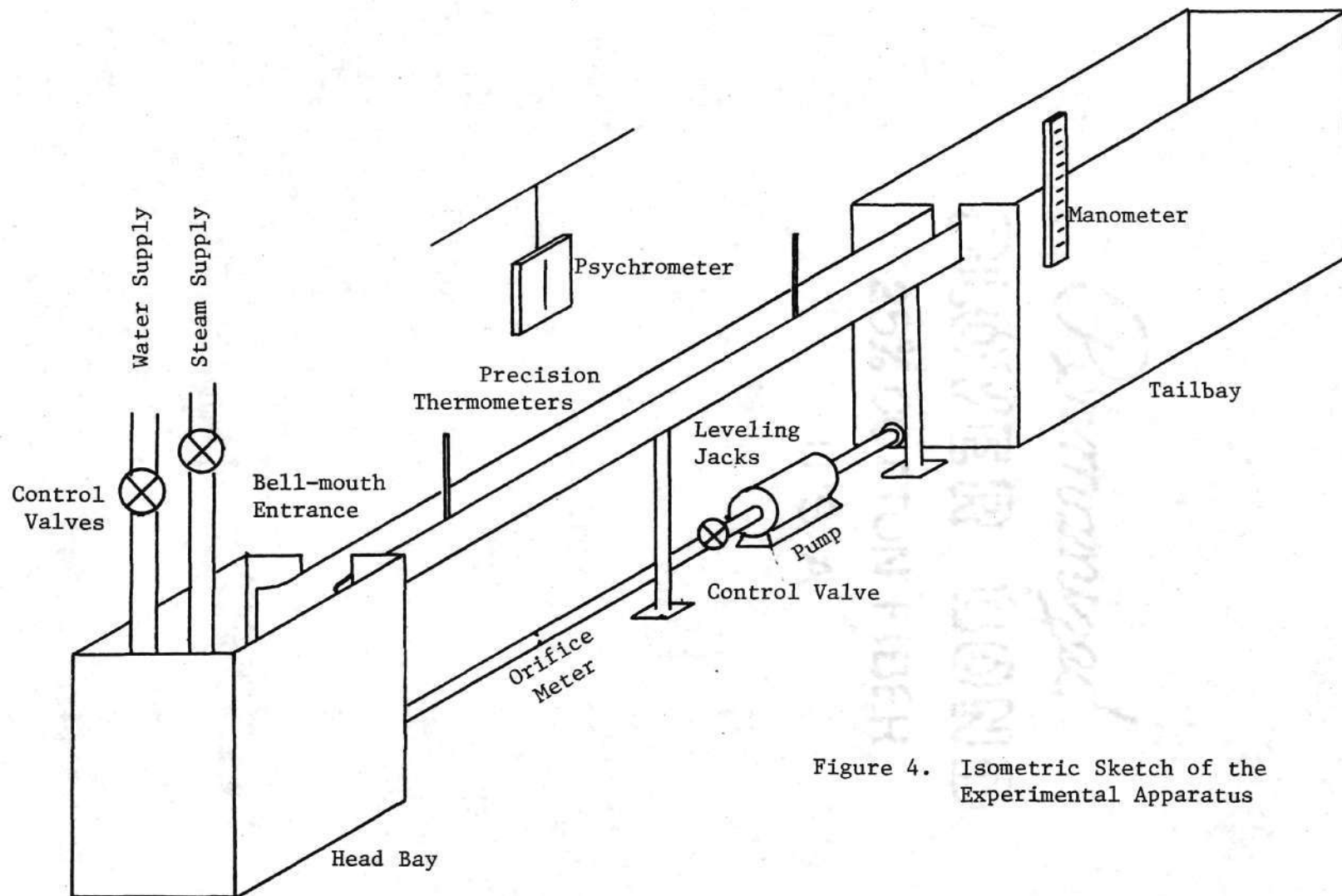


Figure 4. Isometric Sketch of the Experimental Apparatus

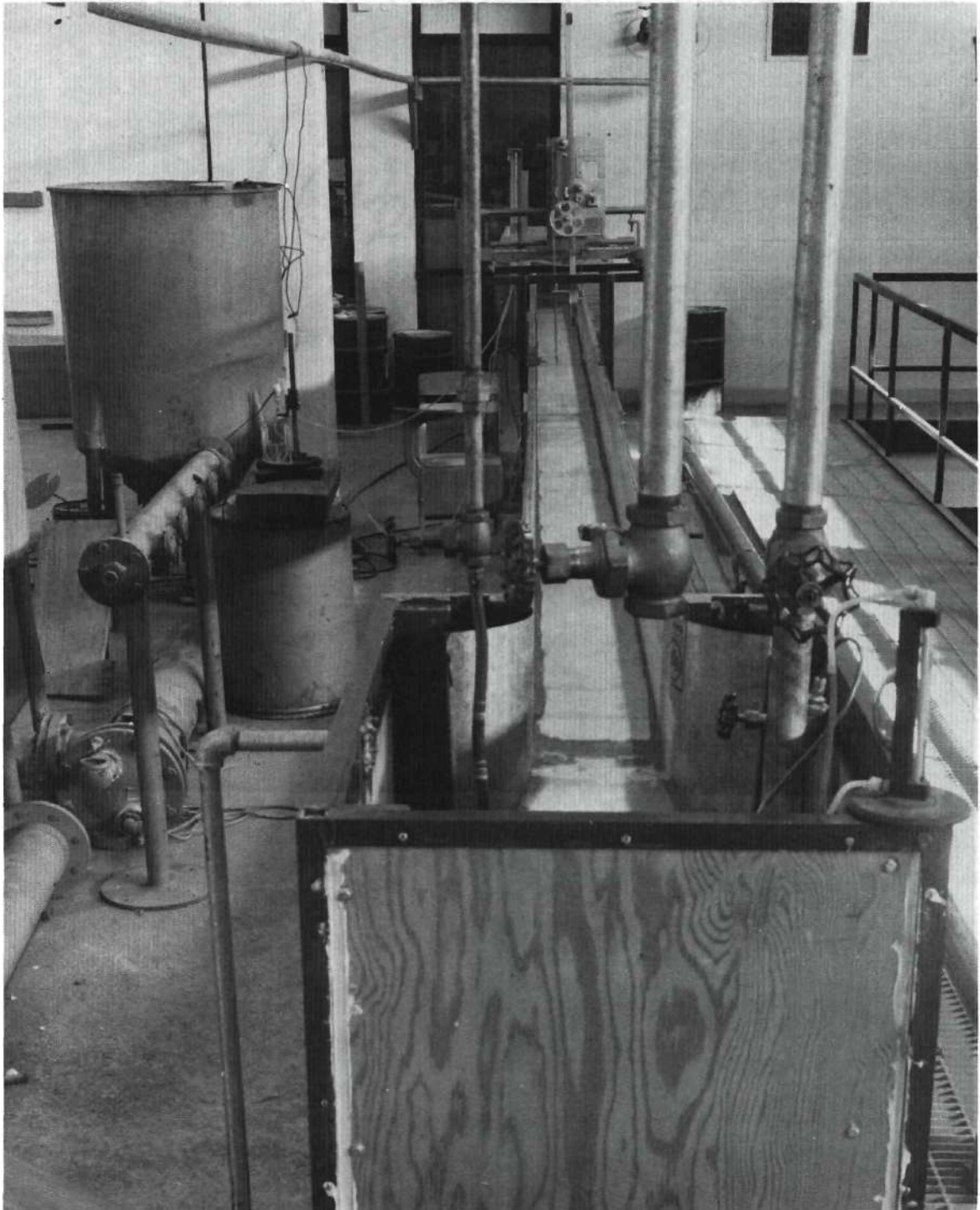


Figure 5. Photograph of Experimental Apparatus, Looking Downstream

water flowing in the artificially roughened flume, and the experiments with heated still water. The artificially roughened flume was created by fastening sections of one-inch aluminum angles to the floor. The roughness elements were oriented at right angles to the flow, staggered longitudinally and placed at stations some eight inches apart.

For the experiments with flowing water, a considerable time was allowed for the establishment of steady-state conditions. A typical experiment would involve the setting of a constant flow rate, a constant water temperature, and constant flow depths. The depth of flow was regulated by an adjustable weir located at the downstream end of the flume. Typical measurements included the water flow rate, the ambient air temperature, the wet bulk temperature, and the barometric pressure. The depths of flow and the bulk temperature of the water were measured at two stations along the flume some twenty feet apart. All measurements were made in duplicate. The flowing water experiments were made at several different volume flow rates, and at several different depths of flow.

For the still water experiments, the flume was sealed off at both ends and filled with hot water. These tests were conducted with several different depths of water. A sufficiently long period was allowed to elapse for the decay of most turbulent eddies introduced during the filling process. The bulk water temperature was then measured at 30-second intervals until the water had cooled approximately 5°C,

CHAPTER V

LABORATORY RESULTS AND ANALYSES

Laboratory Results. As described previously, the net heat flux across an air-water interface depended in a large measure on near-interface temperature gradients. In relatively quiescent open channel flows, these temperature gradients depended on thermal conduction, on thermally induced convection, and on naturally occurring turbulence (Reynolds number effects). These flow conditions were modeled in the laboratory by flows in the smooth-walled flume. In highly turbulent flows, large-scale eddies considerably enhance the already existing mixing. In the completely turbulent flow range, as defined in the hydraulic literature, wall roughness determines the level of turbulent mixing and thus the level of heat transfer. The flow conditions were modeled in the laboratory by the insertion of regularly spaced roughness elements onto the bottom of the smooth-walled flume.

The results of the flowing water experiments are given in Table 1 for the smooth channel, and in Tables 2, 3, and 4 for the rough channel. The results of the still water experiments are given in Tables 5 and 6. Test runs were made with uncovered flumes, covered flumes, and covered flumes with simulated wind conditions in which the air space above the water was continually evacuated by means of a fan (wind tunnel effect). In this report, only the free surface data were analyzed.

Comparison of Free-convection Equation with Still Water Data. The

Table 1. Experimental Data - Smooth Channel

Run #	T _{db} °C	T _{wb} °C	Q gpm	D ₁ in.	D ₂ in.	T ₁ °C	T ₂ °C	Rel. Hum. %	U	C	C/F	Comments
1	23.7	10.0	46	5.813	5.813	58.74	58.51	14	✓			p. 92 notebook
2	23.8	10.6	46	3.813	3.813	57.89	57.85	14	✓			
3	24.0	10.3	46	4.813	4.813	57.29	59.12	14	✓			
4	24.2	10.9	46	5.625	5.625	56.46	56.23	14	✓			
5	23.4	10.4	33	4.937	4.937	56.53	56.39	14	✓			
6	24.4	10.8	33	4.188	4.188	56.86	56.60	14	✓			
7	25.8	11.7	46	5.437	5.437	61.05	60.84	19	✓			p. 96 notebook
8	26.2	13.2	46	5.437	5.437	64.00	63.74	19	✓			
9	26.1	12.6	46	3.937	3.937	64.32	64.14	17	✓			
10	26.1	12.6	46	3.250	3.125	64.32	64.18	17	✓			
11	26.0	12.8	46	4.750	4.750	63.76	63.55	18	✓			
12	26.6	13.0	46	4.750	4.750	64.32	64.13	19	✓			
13	23.8	10.9	36	3.688	3.688	64.50	64.29	16	✓			p. 98 notebook
14	23.9	10.9	36	5.437	5.437	64.21	63.85	15	✓			
15	23.9	10.9	36	4.750	4.750	63.72	63.43	15	✓			
16	24.2	10.7	36	3.937	3.937	63.28	63.04	13	✓			
17	25.4	11.2	36	5.937	5.937	63.99	63.62	12	✓			p. 100 notebook
18	25.4	11.2	36	3.813	3.813	63.83	63.60	12	✓			
19	25.7	11.0	36	5.125	5.125	63.68	63.39	11	✓			
20	25.6	11.0	36	4.625	4.625	63.21	62.90	11	✓			
21	24.2	10.5	46	6.813	6.813	64.02	63.74	10	✓			p. 104 notebook
22	24.2	11.0	46	5.437	5.437	64.53	64.26	11	✓			
23	24.4	12.6	46	3.375	3.375	66.99	66.71	22	✓			(?)
24	24.4	11.6	46	4.250	4.250	66.95	66.66	17	✓			
25	23.9	17.8	46	3.937	4.00	64.25	64.14	55	✓			p. 112 notebook
26	24.1	17.6	46	5.313	5.437	64.08	63.93	53	✓			
27	24.0	17.6	46	6.563	6.625	63.46	63.32	53	✓			
28	24.1	17.4	46	6.063	6.125	64.11	63.97	51	✓			
29	24.3	17.8	46	5.437	5.563	64.66	64.32	53	✓			
30	24.3	17.8	46	4.625	4.750	64.53	64.43	53	✓			

Table 1. Continued - Smooth Channel

Run #	T _{db} °C	T _{wb} °C	Q gpm	D ₁ in.	D ₂ in.	T ₁ °C	T ₂ °C	Rel. Hum. %	U	C	C/F	Comments
1D	25.0	18.2	48	5.437	5.562	64.56	64.42	52				P. 118 notebook
2D	25.2	18.0	47	4.062	4.125	64.79	64.63	49				
3D	25.4	18.0	47	6.250	6.250	63.51	63.39	47				
4D	25.4	17.8	47	5.312	5.437	63.17	63.03	47				
5D	25.4	17.8	48	4.437	4.562	64.00	63.87	47				
6D	23.8	17.2	46	5.250	5.375	63.94	63.64	53				P. 112 notebook
7D	24.1	17.1	46	5.750	5.937	64.33	64.03	49				
8D	24.2	17.8	46	6.437	6.625	64.36	64.09	54				
9D	24.4	18.2	46	3.750	4.875	65.23	65.00	55				
10D	24.4	18.2	46	4.437	4.625	66.01	65.74	55				
11D	24.1	17.8	46	5.187	5.375	66.07	65.79	54				All data U

Table 2. Experimental Data - Rough Channel, Series A

Run #	T _{db} °C	T _{wb} °C	Q gpm	D ₁ in.	D ₂ in.	T ₁ °C	T ₂ °C	Rel. Hum. %	U	C	C/F*	Comments
1A	25.1	15.3	60	4.0	3.875	64.67	64.41	34	✓	✓		*C/F, covered channel with fan.
2A	25.2	16.0	60	4.0	3.875	65.07	64.99	37				
3A	25.4	16.2	60	4.0	3.875	65.14	64.89	37			✓	
4A	25.5	16.9	60	4.813	4.688	65.10	64.80	42	✓	✓		
5A	25.8	16.4	60	4.813	4.688	65.36	65.27	37.5				
6A	25.9	16.4	60	4.813	4.688	65.37	65.11	37			✓	
7A	26.4	21.8	60	5.813	5.688	63.78	63.50	67	✓	✓		
8A	26.8	22.2	60	5.813	5.688	63.89	63.77	67				
9A	27.0	21.8	60	5.813	5.688	63.69	63.45	64			✓	
10A	26.9	23.0	45	5.313	5.250	63.79	63.40	72	✓	✓		
11A	28.0	23.0	45	5.313	5.250	64.14	63.93	65				
12A	28.4	23.0	45	5.315	5.250	64.21	63.81	65			✓	
13A	26.4	22.4	45	4.250	4.125	63.84	63.50	71	✓	✓		
14A	28.2	22.6	45	4.250	4.125	64.37	64.22	62			✓	
15A	28.6	22.4	45	4.250	4.125	64.28	63.95	59				
16A	28.4	23.0	45	3.688	3.313	64.36	64.02	63	✓	✓		
17A	28.4	23.0	45	3.688	3.313	64.67	64.50	55				
18A	28.8	23.6	45	3.688	3.313	64.54	64.18	65			✓	

Table 3. Experimental Data - Rough Channel, Series B

Run #	T _{db} °C	T _{wb} °C	Q gpm	D ₁ in	D ₂ in	T ₁ °C	T ₂ °C	Rel. Hum. %	U	C	C/F*	Comments
1B	26.4	21.0	60	4	3.625	63.91	63.70	61	✓			*C/F, covered
2B	26.6	21.4	60	4	3.625	63.82	63.79	63		✓		channel with fan
3B	27.1	22.3	60	4	3.625	63.82	63.49	66			✓	H (high speed)
4B	27.0	22.2	60	4	3.625	63.90	63.64	66			✓	L (low speed)
5B	27.3	22.8	60	4.5	4.375	64.41	64.16	68	✓			
6B	27.4	22.8	60	4.5	4.375	64.72	64.60	66		✓		
7B	27.4	22.7	60	4.5	4.375	64.55	64.28	67			✓	
8B	27.8	23.2	60	4.5	4.375	63.87	63.52	68			✓	L
9B	26.8	22.0	60	5.75	5.75	63.67	63.41	66				
10B	27.6	22.4	60	5.75	5.75	63.96	63.88	65	✓			
11B	27.5	21.7	60	5.75	5.75	63.58	63.30	60		✓		
12B	27.6	22.2	60	5.75	5.75	63.35	63.16	63			✓	
13B	29.4	22.6	45	5.313	5.313	64.07	63.77	65	✓			
14B	29.4	22.8	45	5.313	5.313	64.46	64.39	57		✓		
15B	29.4	22.2	45	5.313	5.313	64.21	63.72	53			✓	L
16B	29.8	23.0	45	4.188	4.125	64.85	64.56	56				
17B	28.9	21.8	45	4.188	4.125	65.55	65.43	52	✓			
18B	29.2	22.2	45	4.188	4.125	64.08	63.53	64		✓		
19B	27.4	22.2	45	4.188	4.125	64.37	64.02	65			✓	H
20B	29.0	23.7	45	3.563	3.375	64.58	64.30	65	✓			
21B	28.0	22.9	45	3.563	3.375	65.13	65.02	62		✓		
22B	28.4	22.8	45	3.563	3.375	63.52	63.07	60			✓	L
23B	28.0	22.5	45	3.563	3.375	63.35	63.84	58			✓	
24B	29.8	22.6	30	4.875	4.875	64.29	64.08	54	✓			
25B	29.3	22.9	30	4.875	4.875	64.38	63.54	53			✓	H
26B	30.0	22.6	30	4.875	4.875	64.44	63.85	56			✓	
27B	30.0	22.7	30	4.875	4.875	64.57	64.04	66	✓			
28B	30.2	23.3	30	3.750	3.750	64.67	64.49	65		✓		
29B	26.8	21.9	30	3.750	3.750	63.84	63.73	65			✓	L
30B	27.8	22.6	30	3.750	3.750	63.96	63.50	62	✓			
31B	27.5	22.4	30	3.063	2.938	64.84	64.35	60			✓	
32B	28.0	22.7	30	3.063	2.938	64.54	63.94	59			✓	L
33B	28.6	23.2	30	3.063	2.938							
34B	29.2	22.8	30									
35B												
36B												

Table 4. Experimental Data - Rough Channel, Series E

Run #	T _{db} °C	T _{wb} °C	Q gpm	D ₁ in	D ₂ in	T ₁ °C	T ₂ °C	Rel. Hum. %	U	C	C/F	Comments
1E	23.4	13.2	46	5.375	5.312	65.19	64.78	29				P. 128 notebook
2E	23.4	13.2	46	5.250	5.312	64.18	63.85	29				
4E	14.6	8.7	46	5.312	5.250	53.83	53.53	44				P. 130 notebook
5E	15.1	8.2	46	5.312	5.250	54.69	54.44	36				
6E	15.4	7.7	47	3.500	3.187	55.52	55.29	31				
7E	17.4	8.8	46	4.125	4.000	64.04	63.64	29				
8E	17.8	8.9	47	3.500	3.187	65.12	64.71	27				
9E	17.6	8.9	46	5.625	5.750	63.54	63.18	27				
10E	24.1	15.0	46	5.312	5.312	64.59	64.30	43				P. 132 notebook
11E	24.4	15.6	46	4.187	4.187	64.90	64.64	40				
12E	24.4	16.0	46	3.500	3.125	64.46	64.16	41				
13E	24.8	16.7	61	5.812	5.812	63.66	63.43	44				
14E	24.8	17.8	61	4.562	4.437	63.96	63.72	50				
15E	25.0	17.2	61	4.000	3.500	64.07	63.86	44				
16E	25.0	17.9	31	4.625	4.687	64.39	63.95	50				
17E	25.0	18.4	31	3.625	3.625	64.71	64.20	53				P. 134 notebook
18E	26.8	16.0	46	3.500	3.187	64.46	64.22	35				
19E	26.9	16.8	46	5.250	5.312	64.54	64.28	35				
20E	27.0	16.9	46	4.187	4.062	64.91	64.66	35				
21E	27.0	16.9	31	3.687	3.625	65.52	65.02	35				
22E	27.1	17.1	31	4.625	4.687	65.43	64.88	35				
23E	27.3	17.2	30	5.375	5.500	65.37	64.88	35				
24E	27.2	17.2	61	5.812	5.812	64.03	63.80	35				
25E	27.1	17.2	61	4.562	4.437	64.39	63.19	35				
26E	27.2	17.2	61	4.000	3.500	64.88	64.66	35				
27E	23.7	15.6	46	5.312	5.187	46.13	46.01	43				P. 136 notebook
28E	23.5	15.8	46	6.187	6.250	46.46	46.32	44				
29E	23.4	16.0	46	7.000	7.062	46.42	46.27	46				
30E	23.4	16.0	46	7.000	7.125	46.29	46.15	46				
31E	23.7	16.4	46	5.312	5.375	54.97	54.79	47				
32E	23.8	16.4	46	4.125	4.062	55.24	55.06	46				
34E	23.8	16.4	46	3.500	3.187	55.60	55.40	46				All data U

Table 4. Continued - Rough Channel

Run #	T _{db} °C	T _{wb} °C	Q gpm	D ₁ in	D ₂ in	T ₁ °C	T ₂ °C	Rel. Hum. %	U	C	C/F	Comments
35E	24.2	16.7	46	6.562	6.625	55.43	55.20	46				
36E	24.0	16.8	46	5.312	5.375	63.74	63.39	47				
37E	24.1	16.9	46	3.625	3.187	64.34	64.00	47				
38E	24.1	16.8	46	4.187	4.062	64.58	64.24	47				
39E	24.2	16.8	46	7.000	7.062	64.08	63.78	46				
40E	23.6	14.5	46	5.312	5.375	44.15	44.10	36				P. 138 notebook
41E	23.6	14.6	46	6.562	6.625	44.06	44.01	36				
42E	23.4	14.4	66	6.625	6.637	43.84	43.76	36				
43E	23.4	14.3	66	5.500	5.562	43.80	43.74	36				
44E	23.8	14.0	66	5.562	5.562	63.40	63.20	31				
45E	24.0	14.0	66	4.625	4.562	63.15	62.94	31				
46E	23.8	13.8	66	4.000	3.625	62.98	62.76	31				
47E	23.6	13.8	46	5.375	5.375	62.71	62.49	31				All data U
48E	22.8	12.4	46	7.000	7.125	45.59	45.48	27	✓			P. 140 notebook
49E	22.7	12.4	46	7.000	7.125	45.26	45.24	27			✓	
50E	22.8	12.5	46	6.062	6.000	44.82	44.74	28	✓			
51E	22.7	12.1	46	6.062	6.000	44.70	44.70	27			✓	
52E	23.0	12.6	46	5.375	5.312	64.38	64.10	27	✓			
53E	23.0	12.9	46	5.375	5.312	64.92	64.88	29			✓	
54E	23.1	12.9	46	6.875	6.937	65.17	64.84	28	✓			
55E	23.0	13.0	46	6.875	6.937	65.49	65.36	30			✓	
56E	23.1	12.9	46	3.500	3.125	65.07	64.80	29	✓			
57E	23.1	12.8	46	3.500	3.125	65.20	65.18	28			✓	

Table 5. Experimental Data - Still Water

Run #1

<u>Time (pm)</u>	<u>Duration (sec)</u>	<u>T (°C)</u>
10:56:00	0	53.98
53:30	30	53.84
57:00	60	53.73
58:00	120	53.44
58:30	150	53.40
59:00	180	53.30
59:30	210	53.29
11:00:00	240	53.08
11:00:30	270	52.90
01:00	300	52.90
01:30	330	52.81
01:45	345	52.72
02:00	360	52.69
02:30	390	52.54
04:00	480	52.28
04:30	510	52.18
05:00	540	52.07
05:30	570	51.84
06:00	600	51.75
07:00	660	51.62
08:00	720	51.41
09:00	780	51.31
10:30	870	50.94
12:30	990	50.60
13:45	1065	50.41
14:30	1110	50.24
15:00	1140	50.03
15:30	1170	50.10
16:00	1200	50.00
16:30	1230	49.98
17:00	1260	49.82
18:30	1350	49.62
19:00	1380	49.53
19:30	1410	49.48
20:00	1440	49.27
20:30	1470	49.13
21:30	1530	49.00
22:30	1590	48.98
23:00	1620	48.90
24:00	1680	48.87
24:30	1710	48.68
25:00	1740	48.59
26:00	1800	48.42

Table 5. Continued

<u>Time(pm)</u>	<u>Duration(sec)</u>	<u>T(°C)</u>
27:00	1860	48.22
27:30	1890	48.15
28:00	1920	48.03
29:00	1980	47.93
29:30	2010	47.91
30:00	2040	47.80
31:15	2115	47.62
32:00	2160	47.50
33:00	2220	47.28
33:30	2250	47.28
34:30	2310	47.13
35:30	2370	47.00
37:00	2460	46.80
40:00	2640	46.50
41:30	2730	46.23
42:00	2760	46.12
42:30	2790	46.00
43:00	2820	45.98
43:30	2850	45.98
44:00	2880	45.90
44:30	2910	45.88
45:00	2940	45.82
45:30	2970	45.75
46:00	3000	45.66
46:30	3030	45.60
47:00	3060	45.58
47:30	3090	45.49
48:00	3120	45.37
48:30	3150	45.35
49:00	3180	45.31
49:30	3210	45.30
50:00	3240	45.20
50:30	3270	45.00
51:00	3300	45.02
51:30	3330	44.91
52:00	3360	44.90
52:30	3390	44.91
53:00	3420	44.78
53:30	3450	44.71
54:00	3480	44.69
54:30	3510	44.65
55:00	3540	44.63
55:30	3570	44.50
56:00	3600	44.45

Table 6. Experimental Data - Still Water

Run #2		
<u>Time (pm)</u>	<u>Duration (sec)</u>	<u>T (°C)</u>
12:30:00	0	54.80
30:30	30	54.80
31:00	60	54.71
31:30	90	54.59
32:30	150	54.49
33:00	180	54.44
33:30	210	54.31
34:00	240	54.27
35:00	300	54.08
36:00	360	53.92
37:00	420	53.87
38:00	480	53.73
39:30	570	53.55
41:00	660	53.26
42:15	735	53.13
43:00	780	53.12
44:30	870	52.90
45:00	900	52.80
46:00	960	52.62
47:00	1020	52.51
48:00	1080	52.41
48:30	1110	52.38
49:00	1140	52.35
49:30	1170	52.31
50:00	1200	52.24
50:30	1230	52.18
51:00	1260	52.11
52:00	1320	52.01
52:30	1350	51.94
53:00	1380	51.87
53:30	1410	51.81
54:00	1440	51.76
58:30	1710	51.19
59:00	1740	51.20
59:30	1770	51.13
01:00:30	1830	51.01
01:01:00	1860	50.90
01:30	1890	50.82
02:00	1920	50.72
02:30	1950	50.71
03:00	1980	50.75
03:30	2010	50.68
04:00	2040	50.61

Table 6. Continued

<u>Time(pm)</u>	<u>Duration(sec)</u>	<u>T(°C)</u>
05:30	2130	50.49
06:30	2190	50.37
07:00	2220	50.30
07:30	2250	50.25
08:00	2280	50.20
08:30	2310	50.10
09:00	2340	50.07
09:30	2370	50.03
10:00	2400	50.01
11:00	2460	49.90
12:00	2520	49.80
13:00	2580	49.70
14:00	2640	49.57
15:00	2700	49.43

Permanized
Plover Bond
25% COTTON FIBER
MADE IN U.S.A.

still water data comprise results of five tests made with the free surface flume sealed at both ends, filled to different depths with hot water (about 53°C) and then allowed to cool. The mean water temperature was measured approximately every thirty seconds until the water cooled about 5°C. To evaluate the heat transfer per unit surface area of water as a function of temperature, $h(T)$, a polynomial function, $T(t)$, was fitted through the data points of water temperature versus time. The heat transfer rate, $h(t)$, as a function of time is then

$$h(t) = -\rho c_p d \frac{dT}{dt} \quad (44)$$

with d the depth of the water and c the heat content. The function $\frac{dT}{dt}$ was evaluated for different temperatures, T , and these values were used to obtain a polynomial approximation to $h(T)$ using the method of linear least squares. The data and polynomial fits are presented in Figures 6 and 8. Direct comparisons were then made between the observed function $h(T)$ and the equation derived in the previous chapter for the heat transfer rate as a function of surface water temperature. As the Figures 7 and 9 show, there is good agreement over the entire range of temperatures. Although a consistent 10% difference between the measured and observed values is evident, it was not thought to be an experimentally significant discrepancy. This difference is overshadowed by the fact that the form of the two curves is very similar over the complete range of data.

It should be noted that the comparisons were made by assuming that the surface temperature was identical to the bulk water temperature. Since these surface temperatures are likely somewhat lower than those

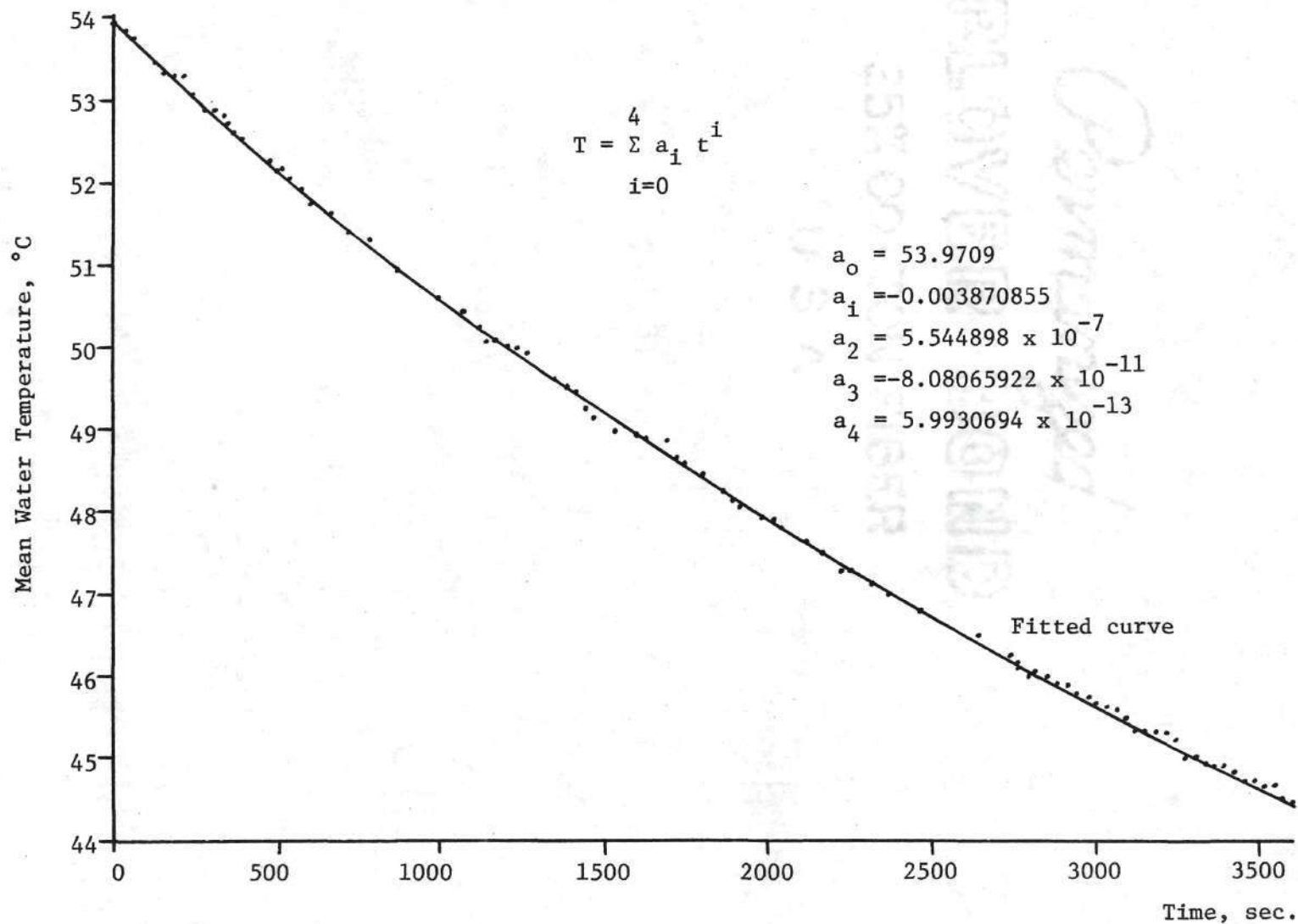


Figure 6. Still Water Cooling Data, Run No. 1

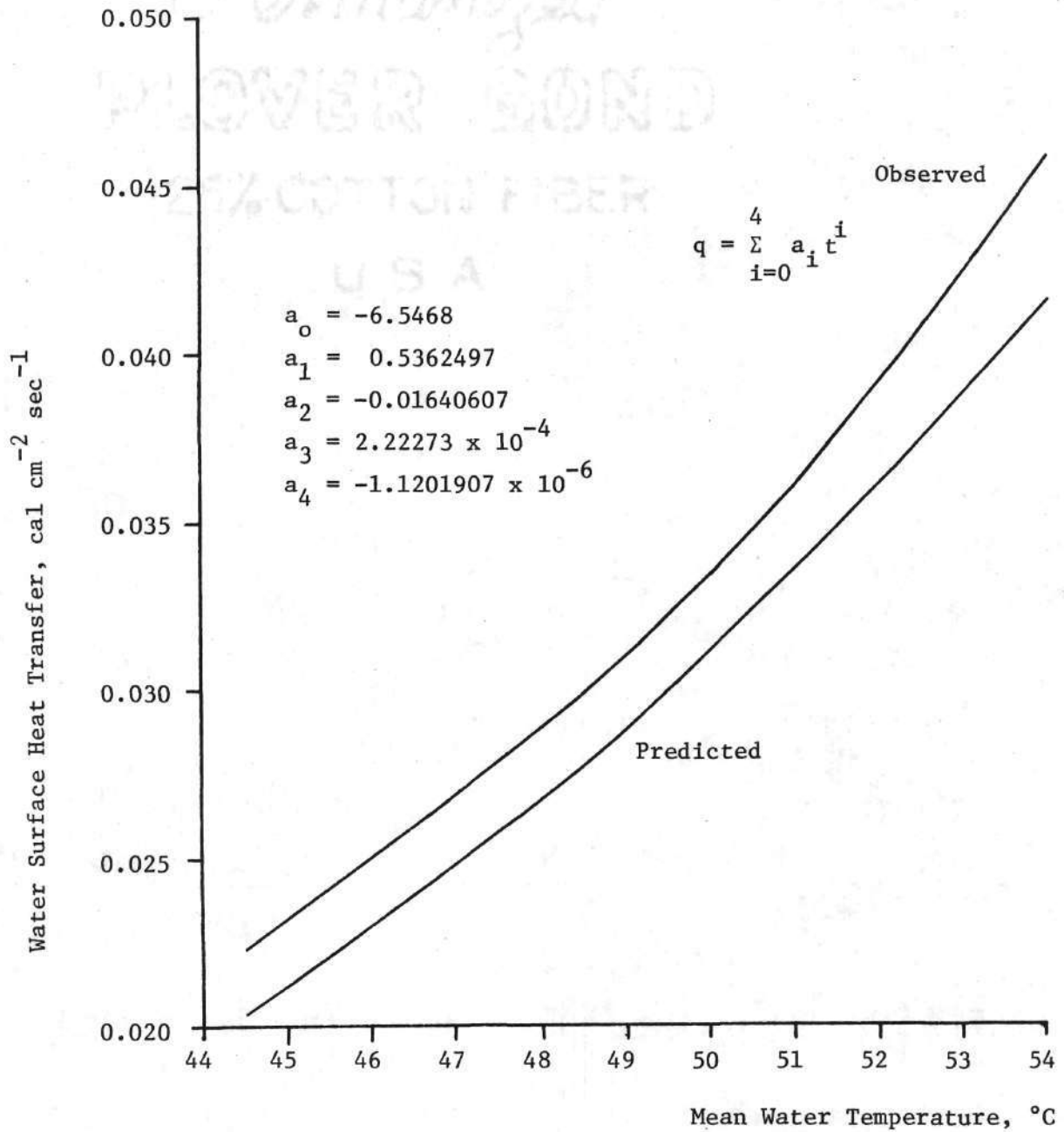


Figure 7. Observed and Predicted Heat Transfer Rates for Still Water, Run No. 1

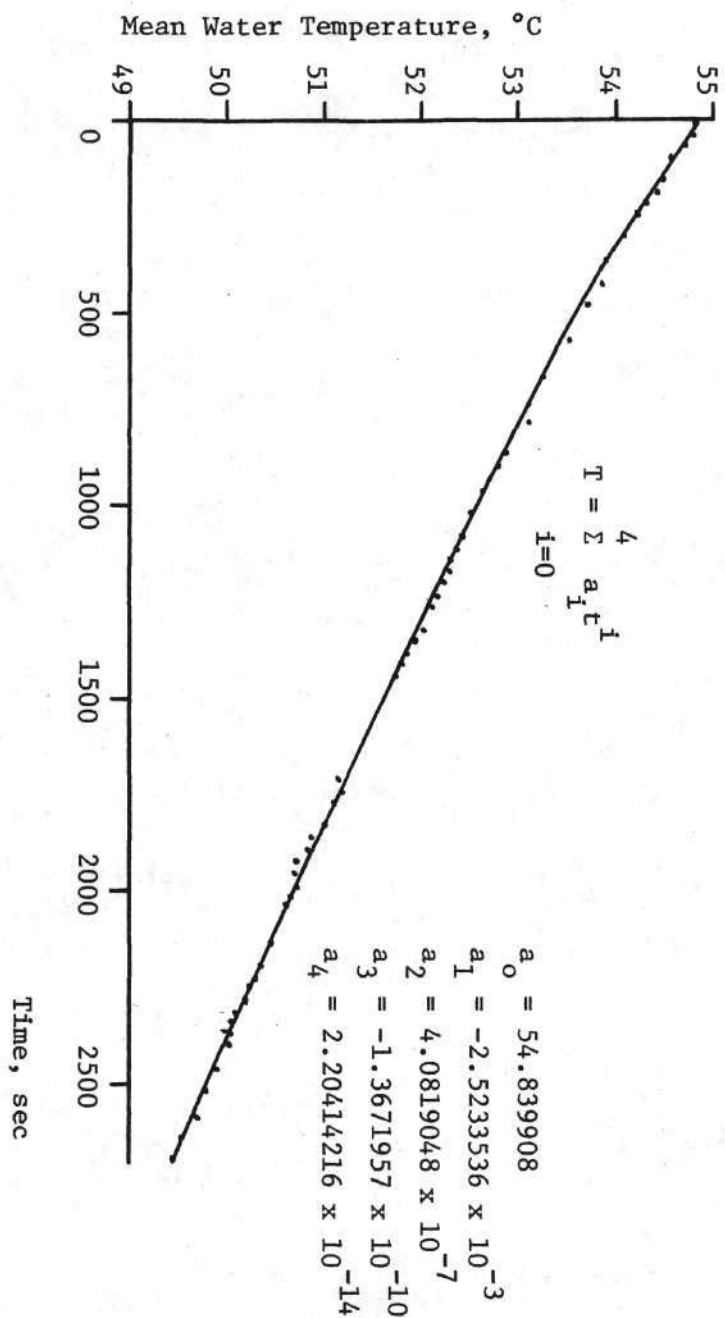


Figure 8. Still Water Cooling Data, Run No. 2

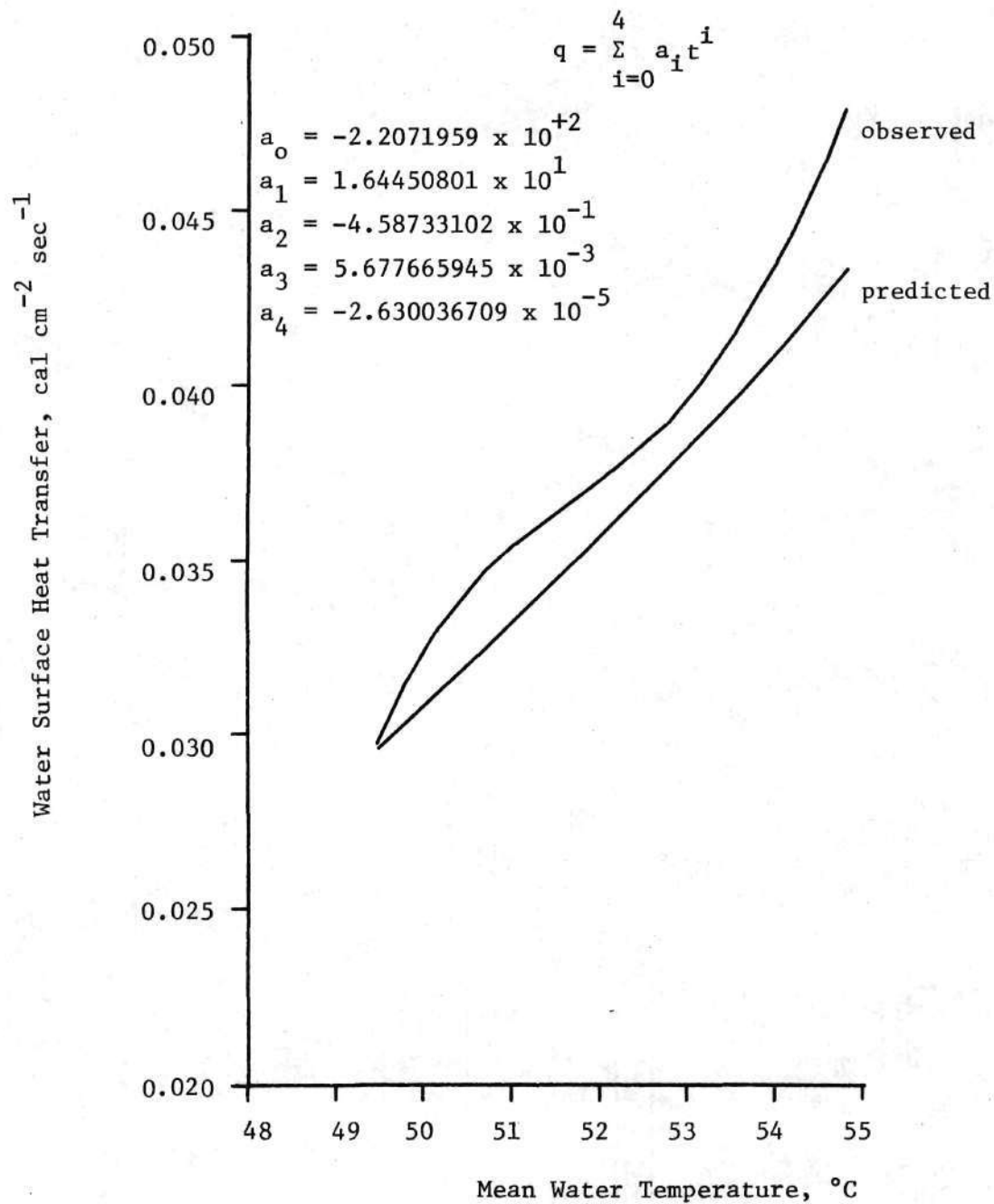


Figure 9. Observed and Predicted Heat Transfer Rates for Still Water, Run No. 2

obtained during the flowing water experiments, it is expected that the surface temperature depression is a great deal smaller. The comparison of the equations in fact seems to depict a surface temperature elevation. This may be also attributed to experimental error in the coefficient of the empirical heat loss equation.

Due to the inability to use the heat transfer equation to determine the surface temperature depression, no comparisons could be made of the experimental results with the Bénard convection equation. The Bénard equation will be later used together with the coefficient obtained from the literature in order to evaluate its relation with results given in the case of flowing water.

Application of Prediction Equation to Smooth and Rough Channel Runs.

The smooth and rough channel heat transfer runs were made with varying laboratory conditions. The mean temperature of water for the majority of runs was between 62° and 64°C . This quantity appeared to be the single most important one affecting the heat transfer rate from the water surface under laboratory conditions. Due to similarity in water temperatures for both the smooth and rough channel data, a meaningful comparison could be made of the effects of channel roughness and hence increased turbulence on the heat transfer mechanism in a flowing stream of water.

The heat transfer rate per surface area for water flowing through the rectangular flume was determined from measurements of the mean water temperature at an upstream and a downstream point to give the total temperature difference between the two points. The product of

this difference, the volume flow rate of the water, and specific heat of water gave the total advected heat loss through the surface between the two measurement points, considering that only a negligible proportion of heat is lost through the wooden channel walls. The heat transfer value obtained divided by the water surface area between the measurement points gives the loss rate per unit surface area.

As shown in Figure 10, a control volume which comprised the entire test section of the flume was used to provide both a visual and a mathematical description of the heat transfer phenomenon. Thus, the only heat fluxes were through cross sectional areas at the ends of the test flume and out the top surface. Applying the continuity to the heat flow gives

$$H_1 - H_2 = H_s \quad (45)$$

and

$$H_s = (T_1 - T_2) \rho_c Q = \rho_c Q \Delta T \quad (46)$$

where Q is the volume flow rate of water. The heat loss per unit surface area, q , is then given by

$$q = H_s / wL \quad (47)$$

Since H_s is evenly distributed over the surface

$$q = \rho_c Q \Delta T / wL \quad (48)$$

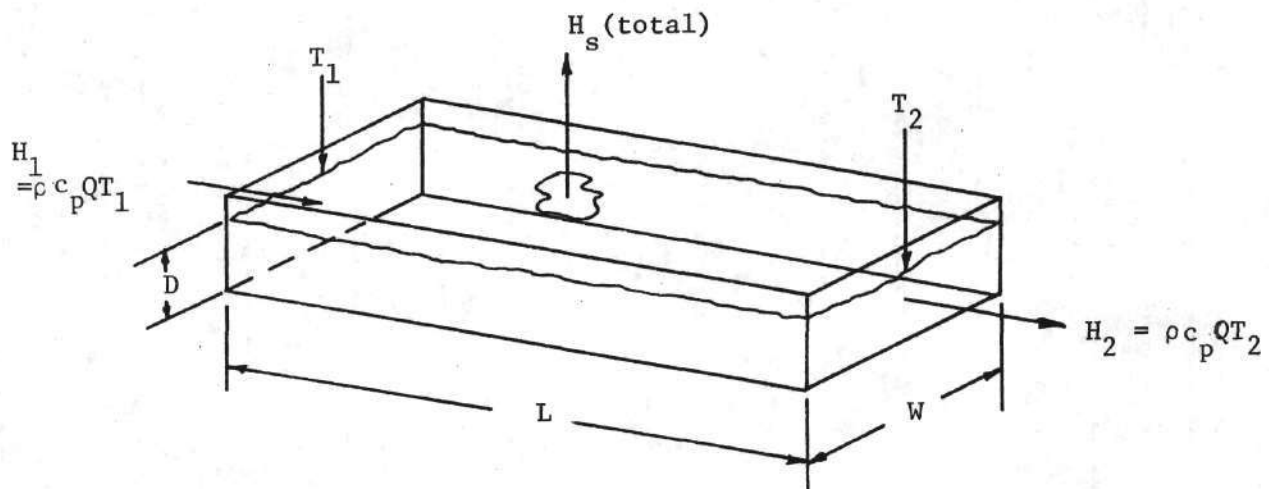


Figure 10. Control Volume for Conservation of Thermal Energy in Flume

The overall temperature drop is thus

$$\Delta T = \frac{wLq}{\rho c_p Q} \quad (49)$$

As long as the volume flow rate remains the same and the surface heat loss does not vary, there will be no variation in ΔT with velocity of flow or depth.

The main premise of this investigation was that by maintaining a fixed volume flow rate, the surface heat loss per unit area can be increased through increased turbulence by varying the velocity and depth of flow as well as by addition of channel roughnesses. The predicted values of the surface heat transfer were computed using Equation 16 and were compared to the experimentally determined values for the rough channel case. These computed values are plotted against the observed values in Figure 11. These predicted values were consistently higher than the observed values. This was expected because the bulk water temperature was used as an estimation of the water surface temperature. Figure 11 then shows that the prediction equation indeed gave reliable results for the rough channel flows at the elevated temperatures.

A next step in the analysis of the rough channel data was to determine what the surface temperatures should have been in order that the predicted transfer rate corresponded with the measured values. An iteration procedure was used to pick trial values of T_s and compare the heat transfer thus predicted with the heat transfer observed. From the converged values of surface temperatures, the predicted surface temperature depression or the difference between the bulk and surface temperatures was obtained. The mean difference obtained was 2.2°C.

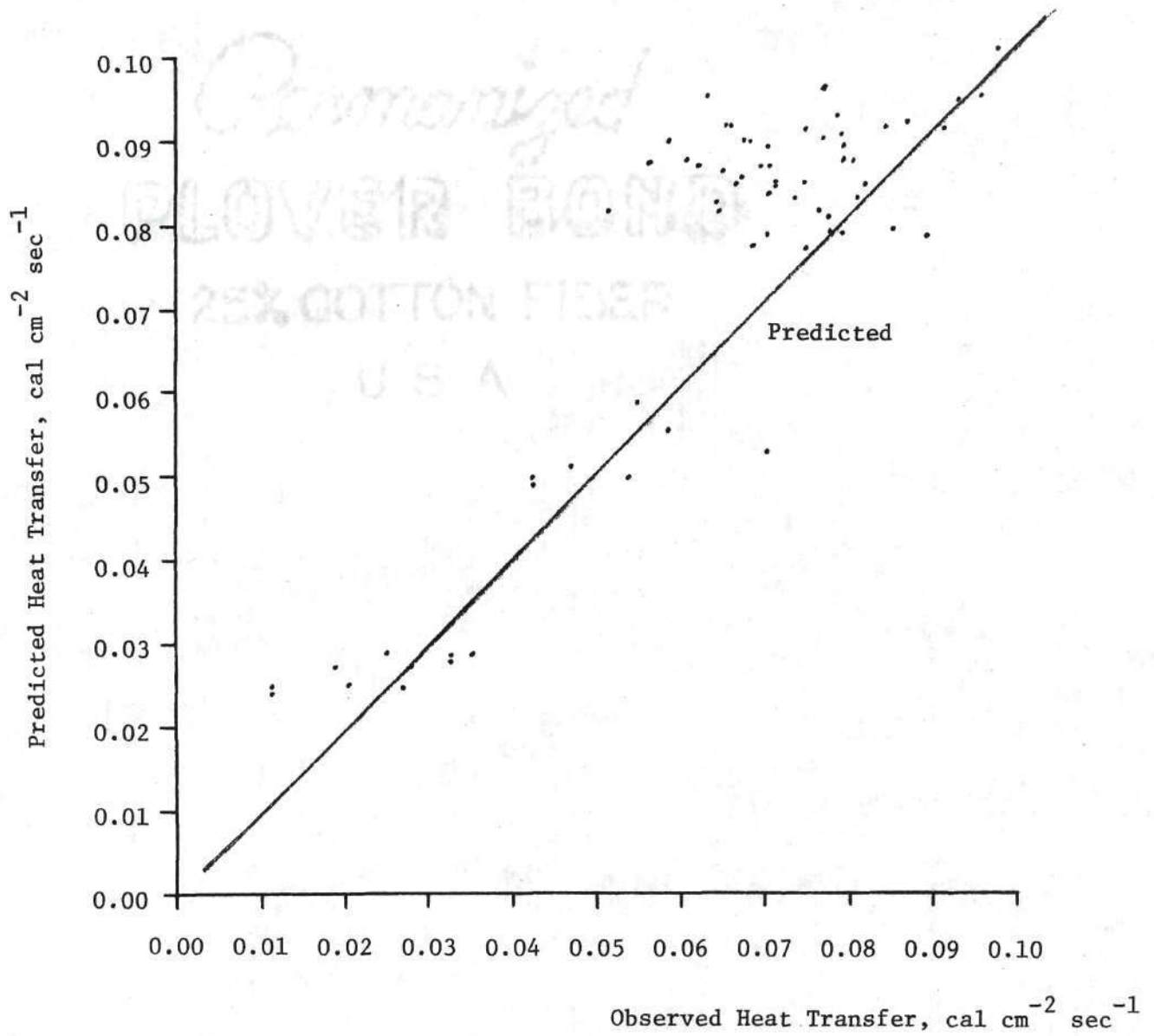


Figure 11. Predicted vs. Observed Heat Transfer in Roughened Channel

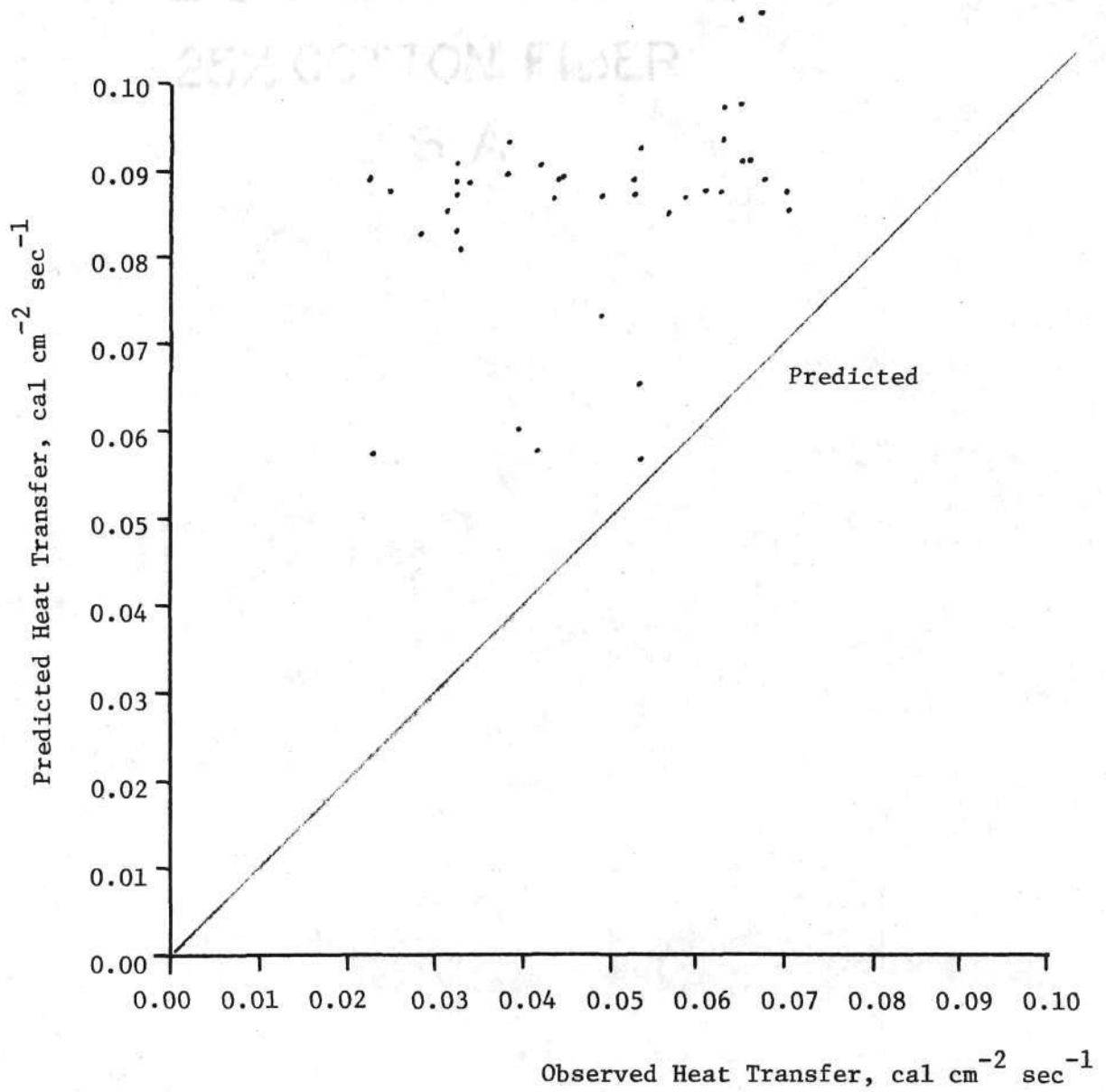


Figure 12. Predicted vs. Observed Heat Transfer in Smooth Channel

The same analysis procedure was applied to the smooth channel data to obtain a comparison. Figure 12 shows the correlation between the predicted and actual values of the surface heat transfer. This figure is analogous to Figure 11. The Figure 12 indicates that the surface temperature depression was significantly larger in the smooth channel than the surface temperature depression in the rough channel. The mean difference between the bulk and surface temperatures was 9.5°C . Figures 13 and 14 present histograms of the computed surface temperature depressions for the rough and smooth channels.

The Figures 11 and 12 show that at similar bulk water temperatures, the more strongly mixed flows exchange more heat to the atmosphere. To obtain quantitative estimates of the effects of mixing on heat transfer, an expression involving the heat transfer rate, the surface temperature depression, the relative roughness of the channel and the intensity of mixing can now be developed from the data. A theoretical derivation of the form of such an expression was presented in Chapter III, Equation 43. In order to apply this expression, an estimation of the equivalent sand grain roughnesses of the channel must be made. These roughnesses were not experimentally determined from hydraulic measurements on the flume itself, but information in the literature allow accurate estimates to be made.

The equivalent sand roughness of smooth wooden flumes was reported to be between 0.0006 and 0.003 feet. Since the flume was smooth, a value of 0.001 feet (approximately .03 cm) was used. Schlichting reported experiments on artificially roughened metal plates using different shapes and arrangements of roughness elements,

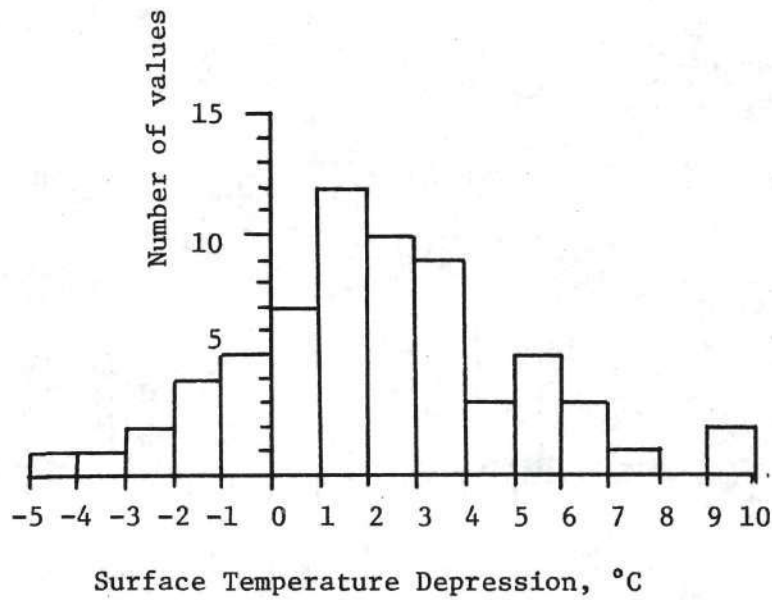


Figure 13. Histogram of Roughened Channel Surface Temperature Depression, Experimental Results

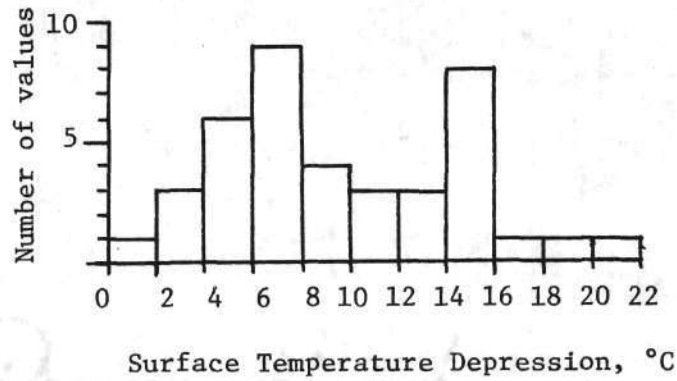


Figure 14. Histogram of Smooth Channel Surface Temperature Depression, Experimental Results

including short angles similar to the roughened flume used in this study. Although using smaller angles than the ones in this study, but with the same spatial arrangement, Schlichting showed that the equivalent sand grain roughness was nearly equivalent to the actual height of the angular protrusion. This observation was used here as an estimate of the roughness of the artificially roughened flume. The height of the angles used was 2.5 centimeters.

Using these values of the roughness height for the smooth and rough channels together with the observed values of the parameters contained in Equation 43, estimates of the coefficient A in the equation were obtained. The mean values were 0.060 and 0.054 respectively demonstrating good agreement with the model when considering the substantial difference in surface roughnesses. The mean value of the coefficient based on the smooth and rough values is then 0.057.

A second determination of the coefficient was made for data points with bulk temperatures between 62 and 65°C only, and then taking the mean of the coefficients. This was considered a more reliable estimate. The values obtained thus were 0.090 for rough channel and 0.11 for smooth channel for an average of 0.10.

CHAPTER VI

APPLICATION OF THE RESULTS

Utilizing the Models. The expressions developed for the determination of heat transfer rates for a number of hydraulic situations related the heat transfer rate, q , to the surface temperature, T_s , and the surface temperature depression, ΔT , to the heat transfer rate. Thus,

$$q = f(T_s) \quad (50)$$

$$\Delta T = T_w - T_s = g(q) \quad (51)$$

giving

$$q = f(T_w - g(q)) \quad (52)$$

where T_w is the bulk water temperature. Determination of q is then seen to involve an iterative procedure, assuming first that $T_s = T_w$, determining q , ΔT , then q , ΔT , etc., until the process converges. The iteration algorithm is

$$\begin{aligned} T_{s1} &= T_w \\ i &= 1 \\ (\text{LOOP}): \quad i &= i + 1 \\ q_i &= f(T_{si}) \\ \text{If } q_i &\text{ is close enough to } q_{i-1} \text{ END} \\ \Delta T_i &= g(q_i) \\ T_s &= T_w - \Delta T_i \quad (\text{LOOP}) \end{aligned} \quad (53)$$

The function g has two distinct forms. The first is for still water and the other for turbulent flowing water. These functions, taken from equations 20 and 43 are

$$\text{still water} \quad g_s(q) = \Delta T = \left[\frac{q}{c_p c_p} \left(\frac{v}{2} \right)^{1/3} \right]^{3/4} \quad (54)$$

$$\text{flowing water} \quad g_f(q) = \Delta T = \frac{[2.5 \ln(12.18R/k)]^{3/2}}{A_p c_p} \left(\frac{\sigma}{\rho D} \right)^{1/2} V^{-3/2} q \quad (55)$$

To demonstrate the use of the predictive models and to give an idea of how the heat transfer varies under the influence of different hydraulic conditions, some examples are given. In these examples, the values of the atmospheric parameters were held constant in order to simulate laboratory conditions, as no short-wave incident radiation heating was included. The heat transfer was computed over the same range of bulk water temperatures for different hydraulic conditions. The examples included still water along with flowing water conditions using different velocities, hydraulic radii, and roughnesses. The atmospheric parameters used in the examples are

Air temperature	25°C
Relative humidity	50%
Wind velocity	0

The values for the total heat transfer and surface temperature depression from these examples are plotted in Figures 15, 16, 17 and 18. The bounding values of heat transfer for the cases of still water and water in which turbulent mixing is sufficient to drive the surface temperature up to average water temperature ($T_s = T_w$) are shown in the figures as dotted lines. These plots show that within these bounds

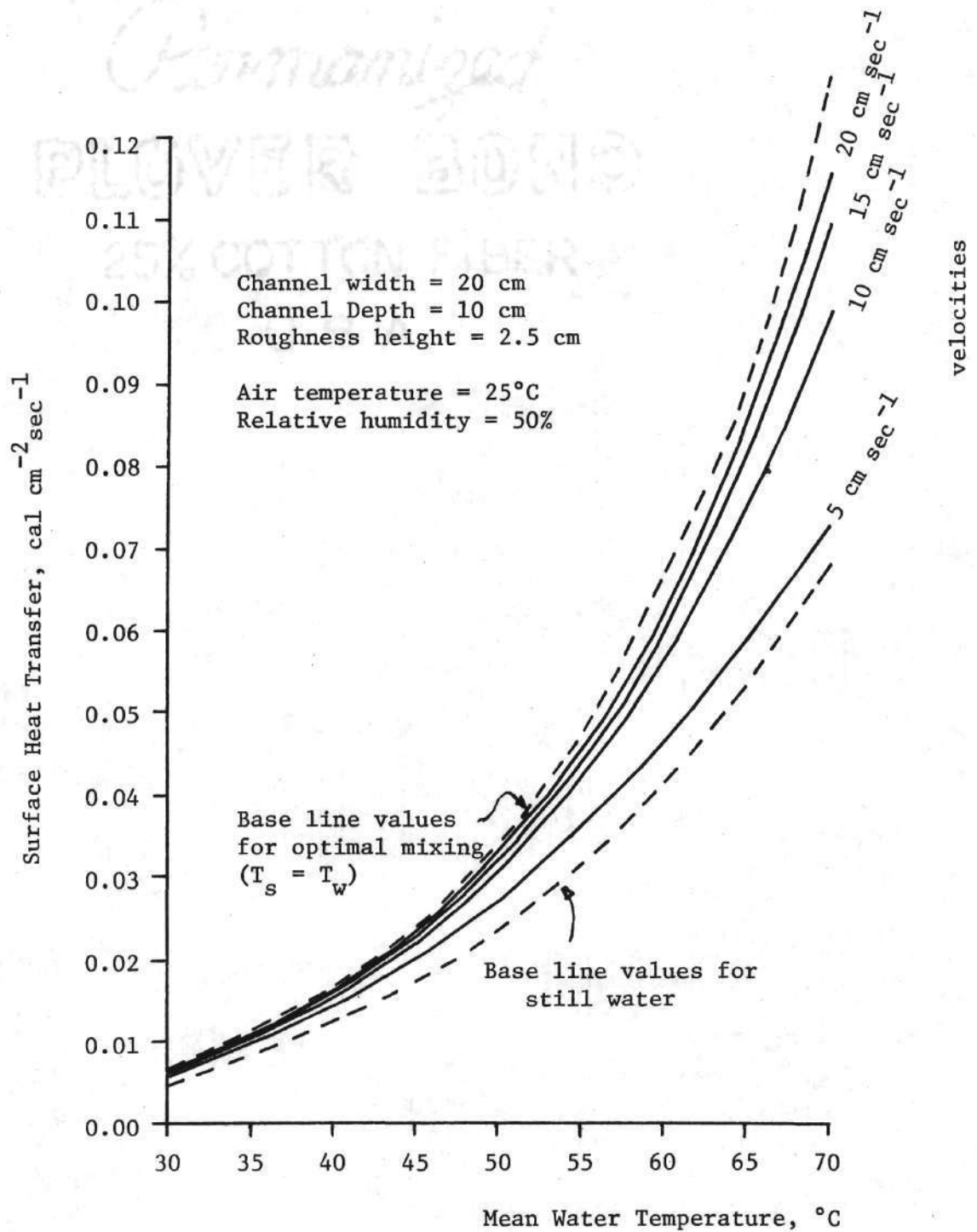


Figure 15. Water Surface Heat Transfer in Roughened Channel

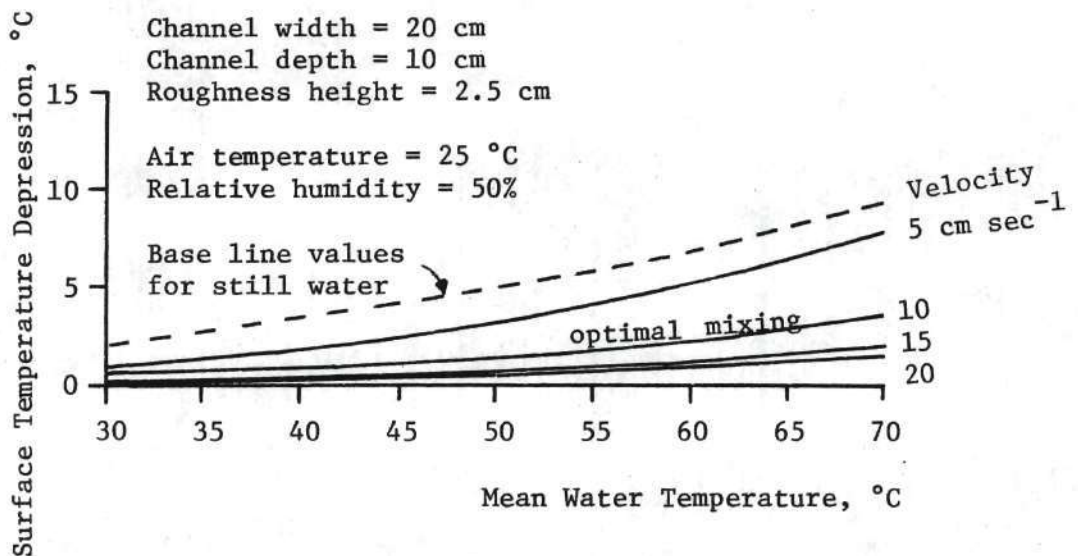


Figure 16. Surface Temperature Depression in Roughened Channel

Permanized

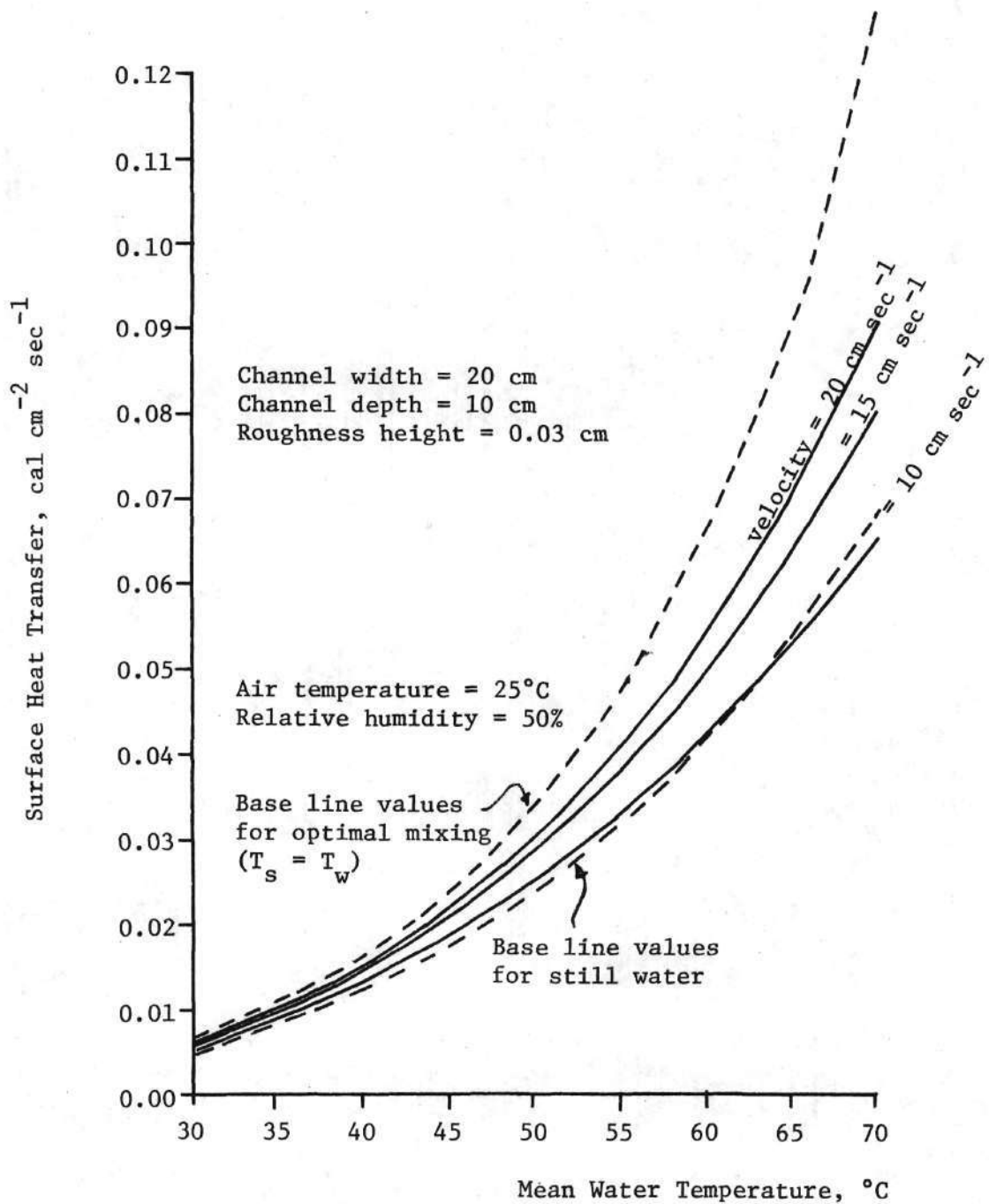


Figure 17. Water Surface Heat Transfer in Smooth Channel

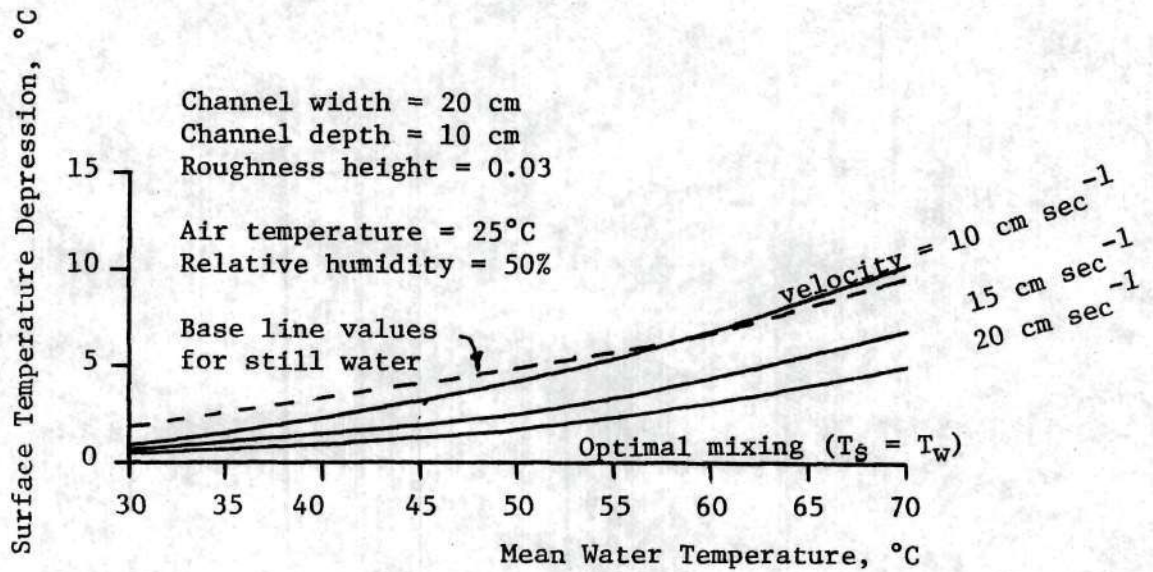


Figure 18. Surface Temperature Depression in Smooth Channel

the overall heat transfer can be increased almost 50% over the amount obtained in the still water case with adequate mixing. In the case of the experimental channel, 20 centimeters wide, 10 centimeters deep and a roughness height of 2.5 centimeters, near-optimal mixing was obtained with a velocity of only 20 centimeters per second. Attempts to further increase the velocity would not significantly increase the heat transfer. Much higher velocities are needed to obtain the theoretical limit of a surface temperature equal to the mean water temperature. The model is, of course, inapplicable at higher velocities where surface stability breaks down. The formation of waves and water spray have a strong effect on the atmospheric boundary layer and on the actual evaporating surface, phenomena which were not considered in the development of the model.

As the lower bound of heat transfer was approached, the effects of Bénard convection became more and more important until a condition was reached at which the internal mixing could not be further retarded by reduction of the flow mixing. The heat transfer cannot be reduced below the lower bound of Bénard convection. The values of velocity, hydraulic radius and roughness height at which this limit is reached gives a working relationship which can be used to provide estimates of the amount of mixing required which will begin to augment the natural thermal convection found in still water. This is an approximate breakpoint between the still water and flowing water convection modes. Examining the different examples near the lower limit, it was found that the inequality

$$\frac{V}{\ln(12.18 R/k)} > 1.3 \quad (56)$$

represents this breakpoint. For values less than 1.3, no heat transfer enhancement is achieved. On the other hand, no more significant increases are obtained with values beyond about 5.0.

Effect on Cooling Pond Design. Traditional cooling pond design is based on the assumption that depth of flow has no noticeable effect on heat transport properties. This notion was probably based on studies conducted on existing ponds whose depths typically varied from 4 to 6 feet. Typical velocities in these ponds were not in the range of values sufficient to augment the natural Bénard convection mixing. The results of this study provide an understanding that the hydraulic conditions in ponds or open channels can be designed so as to provide the turbulent mixing required to reduce the conductive layer thickness and to bring about overall increases in heat transfer. When properly designed, significantly smaller surface areas are required.

Using Equation 48 and assuming constant volume flow rate and temperature drop, and a per surface heat transfer of q , the required surface area is

$$\text{Area} = wL = \rho c_p Q \Delta T / q \quad (57)$$

with an enhanced transfer, $q^* = 1.5q$,

$$\text{Area}_* = \rho c_p Q \Delta T / q_* = \text{Area} / 1.5 = 0.67 \text{ Area} \quad (58)$$

Thus, only two-thirds of the traditional surface area requirement is necessary to obtain the same temperature drop. This substantial saving

can be made possible through decreasing the flow depth and by increasing the channel roughness.

Permanized
FLOVER BOND
25% COTTON FIBER
U.S.A.

CHAPTER VII

CONCLUSIONS AND RECOMMENDATIONS

Conclusions. The study served as an excellent educational experience. Knowledge in areas of fluid mechanics, thermodynamics, and environmental engineering were combined to address the important contemporary problem of thermal pollution. The combined results of the both the laboratory studies and the theoretical considerations can be stated as follows:

- 1) A water surface heat transfer model was developed for the estimation of heat transfer due largely to natural convection of water vapor in the atmosphere. This model gives good results in the range of natural water temperatures and at elevated temperatures encountered in thermal discharges from industrial plants. Use of this model in conjunction with the technique developed for estimating the surface temperature depression due to cooling allow a reasonably accurate determination of the heat transfer, and hence the cooling to be expected under given atmospheric and hydraulic situations.
- 2) A study of the effects of channel roughness on the heat transfer from the surface of a turbulent flowing stream revealed that an increased channel roughness results in a significant increase in the overall heat transfer.
- 3) A predictive model of the variation in surface temperature

depression, including the effects of overall heat transfer rate and major hydraulic parameters of the flowing stream, was confirmed by experimental results from smooth channel experiments as one case and rough channel experiments as a second case. The differences, on the average, between these two cases were predicted closely by the model.

- 4) A good correlation between the predictive model and the data within each of the roughness groups on a point-by-point basis was not obtainable due to the experimental spread of the data. This was largely due to the difficulty of obtaining sufficiently accurate water temperature measurements. Only when considered as a whole were the data from the roughness groups sufficiently significant.
- 5) A classical Bénard convection model for estimation of the surface temperature depression in still water was studied. From this lower limit of mixing a breakpoint was determined showing the minimum amount of turbulent flow mixing required to enhance cooling rates.
- 6) An algorithm was presented for the use of the models developed. This algorithm gave a proposed design procedure for determination of expected heat transfer rates for given atmospheric and hydraulic parameters.

Recommendations. Although this study was reasonably successful, extensive investigations should be made to further define and quantify the influence of channel roughnesses and flow-induced turbulent mixing on the enhanced cooling rates from heated water in open channel flow.

Such studies should analyze the variation of heat transfer with widely varying velocities and depths. The roughness height variation as depicted in the model is fairly well substantiated. Confirmational studies could be conducted with different roughness elements and element spacing. Also, efforts should be made to gain more accurate estimates of the surface heat transfer rate. The upstream to downstream temperature drop method had its drawbacks, including small temperature differences in laboratory studies, and the fact that in the experimental flume, it was an overall transfer value which included portions of the channel with rather large flow acceleration. A point heat transfer estimate, such as a vertical heat flux determination using hot wire anemometry techniques, might lead to more reliable results. In this way, the measurements could be obtained from a channel region most closely approximating uniform open channel flow.

PLOVER BOND

2% COTTON FIBER

U S A

REFERENCES

1. Anderson, E. R., Energy Budget Studies, Water Loss Investigations-Lake Hefner Studies, U. S. Geological Survey Prof. Paper 269, 71, 1954.
2. Barnes, Jr., Harry H., Roughness Characteristics of Natural Channels, Geological Survey Water-Supply Paper 1849, United States Government Printing Office, Washington, 1967.
3. Bénard, H., Les tourbillons cellular dans une nappe liquid, Revue Gen. Sci. Pur. Appl., vol. 11, 1261-1271 (1900).
4. Bowen, I. S., The Ratio of Heat Losses by Conduction and by Evaporation from any Water Surface, Phys. Rev., 27, 779-89, 1926.
5. Chow, Ven T., Open-Channel Hydraulics, McGraw-Hill, New York, 1959.
6. Chu, T. Y., and R. J. Goldstein, Turbulent Convection in a Horizontal Layer of Water, J. Fluid Mechanics, vol. 60(1), 141-159 (1973).
7. Dalton, J., Meteorological Observations. Essays on evaporation, Proc. Manchester Lit. Phil. Sav., vol. 5, 1834.
8. Eagleson, P. S., Dynamic Hydrology, McGraw-Hill, New York, 1970.
9. Federal Water Pollution Control Administration, Industrial Waste Guide on Thermal Pollution, Pacific Northwest Water Laboratory, Corvallis, Oregon, September 1968, 112 p.
10. Fishenden, M., and O. A. Saunders, An Introduction to Heat Transfer, pp. 92-97, Oxford University Press, Oxford (1950).
11. Fujii, T., and H. Imura, Natural Convection Heat Transfer from a Flat Plate with Arbitrary Inclinations, Int. J. Heat Mass Transfer, vol. 15, 755-767 (1972).
12. Hickman, K. C. D., Maximum Evaporation Coefficient of Water, Ind. Eng. Chem. 46, 1442 (1954).
13. Hinze, J. R., Turbulence, pp. 299-302, McGraw-Hill, New York, 1959.
14. Hollands, K. G. T., G. D. Raithby, and L. Konicek, "Correlation Equations for Free Convection Heat Transfer in Horizontal Layers of Air and Water," International Journal of Heat and Mass Transfer, vol. 18, pp. 879-884, 1975.

15. Keulegan, Garvis H., Laws of Turbulent Flow in Open Channels, Research Paper RP 1151, Journal of Research, U. S. National Bureau of Standards, vol. 21, pp. 707-741, December 1938.
16. Kohler, M. A., Lake and Pan Evaporation, Water Loss Investigations-Lake Hefner Studies, Technical Report, U.S.G.S., Professional Paper 269, 1954.
17. Krishnamurti, R., On the Transition of Turbulent Convection, Part 1, The Transition from Two-to-Three Dimensional Flow, J. Fluid Mechanics, vol. 42(2), 295-307 (1970).
18. Krishnamurti, R., On the Transition to Turbulent Convection, Part 2, The Transition to Time Dependent Flow, J. Fluid Mechanics, vol. 42(2), 309-320 (1970).
19. Levich, V. G., Physicochemical Hydrodynamics, pp. 689-699, Prentice-Hall, Inc., Englewood Cliffs, New Jersey.
20. Malkus, W. V. R., Discrete Transitions in Turbulent Convection, Proc. Roy. Soc., Sev A, 225, 196, 1954.
21. Mangarella, P. A., Chambers, A. J., Street, R. L., and Hsu, E. Y., Laboratory Studies of Evaporation and Energy Transfer Through a Wavy Air-Water Interface, Stanford University, Stanford, California, September 21, 1972.
22. Marciano, C. J., and E. G. Harbeck, Mass Transfer Studies, Water Loss Investigations-Lake Hefner Studies, U. S. Geological Survey, Prof. Paper 269, 46, 1954.
23. Mayer, P. G., and M. D. Moss, "Heat Dissipation from Turbulent Open Channel Flow," Proceedings, First International Congress on Water Resources, Chicago, Illinois, September 1973.
24. Morris, Jr., Henry M., A New Concept of Flow In Rough Conduits, Transactions, American Society of Civil Engineers, vol. 120, pp. 373-398, 1955.
25. O'Toole, J. L., and P. L. Silveston, Correlations of Convective Heat Transfer in Confined Horizontal Layers, A.I.C.H.E., Chem. Engng. Progr. Symp. Ser., vol. 57(32), 81-86 (1961).
26. Pailey, P. P., Enzo O. Macagno, and John F. Kennedy, Winter-regime Surface Heat Loss from Heated Streams, Iowa Institute of Hydraulic Research, Report No. 155, University of Iowa, Iowa City, March 1974.
27. Raphael, Jerome M., Prediction of Temperature in Rivers and Reservoirs, Proc. Amer. Soc. Civ. Engr., J. of Power Div., pp. 157-181, vol. 88, no. P02, July 1962.

28. Robinson, A. R., and M. L. Albertson., Artificial Roughness Standard for Open Channels, Transactions, American Geophysical Union, vol. 33, no.6, pp. 881-888, December 1952.
29. Rohwer, C., "Evaporation from Free Water Surfaces," U. S. Department of Agriculture, Technical Bulletin No. 271, December 1931.
30. Ryan, P. J., Donald R. F. Harlemann, and Keith D. Stalzenbach, "Surface Heat Loss from Cooling Ponds," Water Resources Research, vol., 10, No. 5, pp. 930-938, 1975.
31. Schlichting, H., Boundary Layer Theory, translated from the German by J. Kesfin, McGraw-Hill, New York, 1955.
32. Shulakovskiy, L. G., "Formula for Computing Evaporation with Allowance for Temperature of Free Water Surface," Soviet Hydrology Selected Paper, No. 61, 566, 1969.
33. Willis, G. E., and J. W. Deardorff, Confirmation and Renumbering of the Discrete Heat Flux Transitions of Malkus, Physics of Fluids, vol. 16(11), 1818-1825 (1973).